VELOCITY MEASUREMENTS WITH A NEW PROBE IN INHOMOGENEOUS TURBULENT JETS

Thesis by

Ivar H. Tombach

In Partial Fulfillment of the Requirements
For the Degree of
Doctor of Philosophy

California Institute of Technology
Pasadena, California

1969

(Submitted May 20,1969)

ACKNOWLEDGMENTS

The author wishes to express his gratitude to his advisor, Professor Anatol Roshko, for his helpful guidance and generous encouragement during the course of the research leading to this thesis. The assistance of Professor Donald Coles, who suggested the heat pulse probe concept and who introduced the author to digital data handling, is also appreciated.

Special thanks go to Mr. Grant Snellen for his indispensable assistance during the digital computation portions of the research. Thanks also go to Mr. Lewis Balthasar, Mr. Raymond Wagoner, and Mr. Robert Davey for their assistance in the construction of the experimental apparatus. The generous cooperation of Mrs. Geraldine Krentler, who typed the manuscript, is also gratefully acknowledged.

The author is indebted to the California Institute of Technology, the National Science Foundation, and the Northrop Corporation for their financial assistance during the many years of study. The research was supported mainly by the Office of Naval Research.

Finally, for her patience, encouragement, and assistance, the author expresses his deepest gratitude to his wife, Evelyn.

ABSTRACT

Velocity profiles have been measured in subsonic, inhomogeneous, axisymmetric turbulent jets, using a new velocity measuring probe. This probe creates a train of heat pulses at one point in the flow and measures the time interval between the time a pulse is created and the time at which it is convected by the flow past a sensing wire a short distance downstream. In a turbulent flow the detected pulses are highly disturbed, but reconstruction of a mean pulse, by a digital computer, from several hundred pulses enabled calculation of a mean velocity and a velocity fluctuation level.

Measurements were made with this probe from near the nozzle to 48 diameters downstream in several combinations of jet gas and ambient gas (air-air, air-He, He-air, and He-SF_6) having a range of jet/ambient density ratios from 0.03 to 7.25. Axial profiles of the variation with the density ratio of the jet width, mean velocity, and turbulence level were obtained from these measurements, showing the entrainment and approach to homogeneity of the inhomogeneous jet. A jet which is less dense than the ambient fluid is seen to entrain the ambient fluid more vigorously than the denser jet, as is demonstrated by its higher turbulence levels, more rapid growth, and more rapid axial decay of the mean velocity.

TABLE OF CONTENTS

TABLE OF CONTENTS (cont'd.)

TABLE OF CONTENTS (cont'd.)

LIST OF TABLES

LIST OF FIGURES

I. INTRODUCTION

The turbulent shear layer between two streams of different densities has been the subject of considerable study in the last few years. This type of flow is important, from an applied point of view, because of its appearance in such applications as jet and nuclear rocket exhausts. It also has an intrinsic interest as a phenomenon in turbulent mixing. The different densities, in addition to having an influence on the processes in the flow, can in many cases act as an identifying label for the origin of the fluid in any point in the flow.

Research in this area began quite some time ago. Corrsin studied an axisymmetric heated jet of air with a hot wire (Refs. 1 and 2) more than twenty years ago. His experiments, with a jet gas to ambient gas density ratio of 0.61 at the nozzle, indicated that the density difference had a negligible effect on the turbulence levels encountered. His measurements of the various temperature and velocity correlations verified directly that the lateral turbulent heat transfer is significantly greater than the lateral momentum transfer, which is displayed by a mean temperature profile which is wider than the mean velocity profile. Corrsin and Uberoi extended this work to other temperatures (Ref. 3), obtaining jet/ambient gas density ratios as small as 0.5.

Mean velocity and composition profiles for circular jets with jet/ambient density ratios ranging from 0.14 to 1.57 were investigated by Keagy and Weller (Ref. 4). Their study of a 0.128-inch diameter jet with a 0.03-inch combination sampling probe and pitot tube showed that the cross-sectional profiles of mean concentration and mean velocity exhibit the same type of similarity in inhomogeneous jets as in homogeneous ones (e.g., the normal probability curve). In all cases the concentration profile was wider than the velocity profile, the difference being the least for the ratio of 0.57 and the greatest for the ratio of 0.14.

Density differences also occur when supersonic jets flow into a quiescent medium of the same composition. In such flows the jet gas is denser than the ambient gas. Several investigators have studied such compressible jets, with the consequence that they are the best understood examples of inhomogeneous mixing. One such investigation, by Eggers (Ref. 5), thoroughly surveyed the flow field of a jet exhausting from a nozzle at Mach 2.22 (which gave a density ratio of 1.98). Eggers compared his results with those which would be predicted by various formulations for the eddy viscosity function, and concluded that the common simple assumption, that of an eddy viscosity which is independent of the radial coordinate, is not justified. He also concluded that, at least for the supersonic jet in quiescent air, various models which incorporated a density into the

eddy viscosity function did not necessarily give better correlation with the experimental data. Whether this conclusion is true in general for all density ratios, or whether his density ratio was not sufficiently large to demonstrate any density-related effect in the eddy viscosity, remains to be seen.

A research program was begun at GALCIT several years ago, with the objective of studying the effects of the density ratio on shear layer stability and on the turbulent mixing process through measurements of the mean and fluctuating velocity and concentration components and their correlations. As a first step in such a study, a circular jet flowing into a closed reservoir, containing either the same gas as the jet or a different one, was built. To make the density effects as large as possible, while keeping the operating costs reasonable, the gases chosen were air and helium, which differ in density by a factor of about 7.25.

In such an experimental study of the mixing of two gases, the measurement of both the velocity and density profiles is not an easy task, since nearly all instruments which measure one quantity require knowledge of the other. Since the flows are turbulent, any instrumentation which is used should be able to respond to the rapidly changing flow velocity and density.

The hot wire is a desirable instrument for measurement in turbulent flows because of its small size and fast

response time. Corrsin (Ref. 1) showed that a pair of hot wires of different diameters, placed in close proximity, could be used to determine both the velocity and composition of a stream composed of a mixture of two gases. The usual hot wire relation is King's Law

$$P = k\ \Delta T(A + B\sqrt{Pe}),$$

where P is the electrical power supplied to the wire, k is the thermal conductivity of the gas, ΔT is the difference between the wire temperature and the stream temperature (which remains fixed in a constant temperature hot wire system), Pe is the Peclet number (= Prandtl number x Reynolds number based on wire diameter), and A and B are geometrical constants which can be determined by calibration. The unknowns in a stream composed of a mixture of two gases are then the velocity U and the gas properties k, Pr, and ν. The gas properties can all be expressed in terms of a mole fraction x, so there are only two unknowns, U and x. With two different wire diameters there will thus be two equations for the two wires:

$$P_i = k(x)\ \Delta T_i\left[A_i + B_i\sqrt{Pr(x)\ \frac{Ud_i}{\nu(x)}}\right]$$

where i = 1 and 2 for wires 1 and 2 respectively, which can be solved numerically for x and U. Such a procedure has been used by Conger (Ref. 6) to measure the decay in the concentration of helium injected into grid turbulence in an

air flow.

When this procedure was tried it led to immediate difficulties. The calibration curve of P vs $\sqrt{Pe}$ for a particular wire at a particular overheat in helium did not lie in the ratio k_{He}/k_{air} (≈ 6) above the air calibration curve, as would be expected from the hot wire equation, but was higher by only a factor of about three. This behavior has also been observed by Aihara, Kassoy and Libby (Ref. 7) and was apparently observed by Conger (Ref. 6, p.1).

This peculiar behavior was explained by Kassoy (Ref.8) as being due to thermal slip at the surface of the wire in helium. The relevant expression here is

$$\Delta T_s \propto \frac{2 - \alpha}{\alpha} \, Kn \, \dot{q}$$

where ΔT_s is the temperature jump, α is the thermal accommodation coefficient, Kn is the Knudsen number, and $\dot{q}$ is the heat transfer rate from the wire. For most common gases $\alpha \approx 1$, so that the slip equation reduces to $\Delta T_s \propto Kn \, \dot{q}$, meaning that if $Kn \ll 1$, then ΔT_s is small. For the usual hot wires $Kn < 0.05$, so the slip is negligible.

In helium, however, the thermal accommodation coefficient on platinum is ~ 0.04, meaning that the slip becomes $\Delta T_s \propto \frac{Kn}{\alpha} \dot{q} = O(\dot{q})$, which is quite significant. The effect of the temperature jump is to decrease the apparent temperature gradient at the wire surface, which decreases the measured power, P, required to maintain the wire temperature.

This behavior can be compensated for by calibration in both gases and also in some mixtures (or by making some appropriate guesses about the behavior of ΔT_s in the mixture). The α is very sensitive to surface condition and age, so frequent calibration would be necessary.

Another more serious problem caused abandonment of the dual hot wire technique. It was found that the output from the wire depended not only on the environment to which it was exposed, but also upon the environment to which it had been exposed. The worst case occurs when a wire which has been sitting in helium for an extended period of time is placed in a pure air stream. Several hours are required before the output from the hot wire circuitry has fully returned to a previously obtained air calibration level. It apparently takes this long before all of the helium molecules on the wire surface have escaped.* An instrument whose output is dependent on past history is obviously unacceptable.**

---

* Such a conclusion would lead one to expect an accommodation coefficient near unity for helium, which leaves a paradox. The writer thanks Bob Davey of Caltech, whose recent work with hot wires and films has brought at least this little bit of order to a very strange behavior, which originally seemed completely random.

** Conger apparently did not have this problem, presumably because his wires were usually in an air stream to which had been added only small amounts ($\sim$ 10%) of helium.

The choice available then, was either to use some other gas than helium (at higher cost), to use some other method to achieve a density difference, such as heating (giving a smaller density difference), or to seek some other method for measuring the flow. The latter course was selected.

Kovasznay measured very low mean speeds in a wind tunnel by measuring the speed at which a periodically varying temperature was convected by the flow (Ref. 9). A thin resistance wire was mounted in the stream and was heated by a sinusoidally varying voltage (at 50 Hz). A hot wire downstream from this heated wire could detect the periodic variation of the wake temperature. By moving this hot wire the wavelength of the heat pattern in the wake could be measured, which determined the mean speed. The instrument was usable in the speed range of 1 to 10 ft/sec.

It appeared that a device of similar form could be used to measure higher velocities if the temperature of the front wire was modulated in such a way that the phase shift between the temperature variation at the first wire and the temperature variation at the second wire could be measured. Calculation of the velocity convecting the heat would then be straightforward for a known separation between the wires.

Several probes were built, using various wire sizes and spacings. Sinusoidal heating was soon discarded because extremely fine front wires would have been required to

faithfully follow the driving current at the high frequencies desired for easy measurement of phase differences. The best results were obtained with a very large step rise in driving current, giving as steep a front to the heat pulse as possible. At this time it was discovered that Bauer (Refs. 10 and 11) had already built an instrument along these lines for measuring velocity in a laminar supersonic flow. The development of the probe which is the subject of this thesis benefited from Bauer's experience with his instrument.

II. THE PRINCIPLE OF THE HEAT PULSE VELOCITY SENSOR

2.1 The Solution for the Wake of a Line Heat Source

The nature of the operation of the pulse velocity sensor is best seen by analysis of a very much simplified model. Assume that there exists a line source of heat along the z axis in a fluid flow which moves at a uniform speed U in the x direction. Let the source release heat at a constant rate $\dot{q}$ per unit length starting at time t = 0, and assume that the heat has no effect on the fluid velocity.

The diffusion equation for the temperature, $\theta(x, y, t) = T(x, y, t) - T_\infty$, is

$$\nabla^2\theta - \frac{1}{\alpha}\frac{\partial\theta}{\partial t} = -4\pi s(\vec{r}, t)$$

where $\alpha = \frac{k}{\rho c_p}$ is the thermal diffusivity and s is the source strength. For this problem

$$s = 0 \text{ for } t < 0$$

$$s = \frac{\dot{q}}{4\pi k}\,\delta(x)\,\delta(y) \text{ for } t > 0 .$$

The Green's function for the diffusion equation in two dimensions is (Ref. 12)*

$$g(R, \tau) = \frac{1}{\tau}\, e^{-\frac{R^2}{4\alpha\tau}}$$

Where $R = |\vec{r} - \vec{r}_o| = \left[(x - x_o)^2 + (y - y_o)^2\right]^{1/2}$

---

* The solution for the instantaneous line source also appears in Ref. 13 in a slightly different form.

and $\tau = t - t_o$. This is the response at $(\vec{r}, t)$ due to a unit impulse at $(\vec{r}_o, t_o)$ in the absence of the convective velocity U. The effect of U is to replace the coordinate x by $x - U(t - t_o)$, hence the appropriate Green's function for this problem is

$$g(R, \tau) = \frac{1}{\tau} \exp\left[-\frac{(x - x_o - U\tau)^2 + (y - y_o)^2}{4\alpha\tau}\right]$$

and the solution is

$$\theta(x, y, t) = \int dt_o \int dV_o \; s(\vec{r}_o, t_o) g(R, \tau)$$

$$= \frac{\dot{q}}{4\pi k} \int_o^t \frac{1}{\tau} \exp\left[-\frac{(x - U\tau)^2 + y^2}{4\alpha\tau}\right] d\tau . \quad (1)$$

Evaluation of this integral follows a method similar to the method of steepest descent for complex functions. The significant portion of the integral comes from the region around the peak of the exponential, i.e., where the exponent is a minimum, which occurs at $\tau = \frac{1}{U}\sqrt{x^2 + y^2} = c$, say. Expand the exponent (call it $g(\tau)$) about c:

$$g(\tau) = -\frac{1}{4\alpha\tau}\left[(x - U\tau)^2 + y^2\right]$$

$$= g(c) + g'(c)(\tau - c) + \frac{1}{2} g''(c)(\tau - c)^2 + \ldots$$

Now $g'(c) = 0$ since the minimum of g is at c, while

$$g(c) = -\frac{1}{2\alpha c}\left[x^2 + y^2 - x\sqrt{x^2 + y^2}\right]$$

and

$$g''(c) = -\frac{1}{2\alpha c^3}\left[x^2 + y^2\right].$$

The centerline of the wake is of greatest interest, so the approximation $\frac{y^2}{x^2} << 1$ gives the simpler expressions

$$c \approx \frac{x}{U}$$

$$g(c) \approx -\frac{y^2 U}{4\alpha x}$$

$$g''(c) \approx -\frac{x^2}{2\alpha c^3} = -\frac{U^3}{2\alpha x}$$

Using these, equation (1) becomes

$$\theta(x, y, t) \approx \frac{\dot{q}}{4\pi k}\int_0^t \exp\left\{-\frac{Ux}{4\alpha}\left[\left(\frac{U\tau}{x} - 1\right)^2 + \frac{y^2}{x^2}\right]\right\}\frac{d\tau}{\tau} . \quad (2)$$

Now, if $\frac{Ux}{\alpha}$ is sufficiently large, the peak will be sufficiently narrow so that $\frac{1}{\tau} \approx \frac{1}{c}$ over the significant region of integration. Since

$$\frac{Ux}{\alpha} = Ux\,\frac{\rho c_p}{k} = Re_x Pr,$$

this approximation is valid if $Re_x Pr >> 1$, which means that x must be sufficiently far downstream and U must be sufficiently large.

Evaluation of equation (2) follows simply now, for

$$\theta(x,y,t) \approx \frac{\dot{q}}{4\pi k}\frac{U}{x}\exp\left[-\frac{Ux}{4\alpha}\frac{y^2}{x^2}\right]\int_o^t \exp\left[-\frac{Ux}{4\alpha}\left(\frac{U\tau}{x}-1\right)^2\right]d\tau$$

$$\approx \frac{\dot{q}}{4k\ Pe\pi}\exp\left[-\frac{Pe}{4}\frac{y^2}{x^2}\right]\operatorname{erf}\left[\tfrac{1}{2}\sqrt{Pe}\right]\left\{1-\frac{\operatorname{erf}\left[\frac{1}{2}\sqrt{Pe}\left(1-\frac{Ut}{x}\right)\right]}{\operatorname{erf}\left[\frac{1}{2}\sqrt{Pe}\right]}\right\},$$

where $Pe = (Re_x)(Pr)$ is the Peclet number.

If it is assumed that the heat source is a hot wire then $\dot{q} = \pi k\theta_1\ Nu$, where Nu is the Nusselt number and θ_1 is the overheat temperature of the wire. Then

$$\theta(x,y,t) = \frac{Nu\theta_1}{4}\sqrt{\frac{\pi}{Pe}}\exp\left[-\frac{Pe}{4}\frac{y^2}{x^2}\right]\operatorname{erf}\left[\tfrac{1}{2}\sqrt{Pe}\right] \cdot\left\{1-\frac{\operatorname{erf}\left[\frac{1}{2}\sqrt{Pe}\left(1-\frac{Ut}{x}\right)\right]}{\operatorname{erf}\frac{1}{2}\sqrt{Pe}}\right\}, \qquad (3)$$

where the assumptions have been: (1) $\frac{y^2}{x^2} \ll 1$, (2) $Pe \gg 1$, (3) the heat source does not physically disturb the flow, and (4) the temperature field does not affect the velocity. This equation is the same as that obtained by Bauer in reference 9. The behavior of θ with t at some x and y is sketched in figure 1.

2.2 The Measurement of Velocity

If it were possible to measure θ as a function of time at some point (x, y) then, using equation (3), it would be possible, in principle at least, to solve for the velocity U (which also appears in Pe). Such a solution could only

be carried out if all the properties of the gas were known, so that Nu and Pe/U could be evaluated, and thus is not useful in a flow of unknown composition.

It turns out that it is possible to determine U from equation (3) without detailed knowledge of the fluid properties. Before proceeding with this, however, it is interesting to note another procedure which can be used.

Bauer (Ref. 10) shows that, if θ is sensed by an uncompensated, constant-current hot wire with a characteristic time constant which is long compared to the rise time of the heat pulse ($\sim \frac{4t_o}{\sqrt{Pe}}$ from Fig. 1), the details of the rise in the stream temperature are unimportant. The wire temperature $\theta_w(t)$, is essentially zero before the temperature rise and rises linearly for some time afterward, as shown in the sketch. Extrapolation of the linear curve down to the t-axis gives the point where $t = t_o = x/U$, with good accuracy. Thus, from a plot of θ_w versus t at some known distance downstream, $x = \ell$, the velocity is obtained

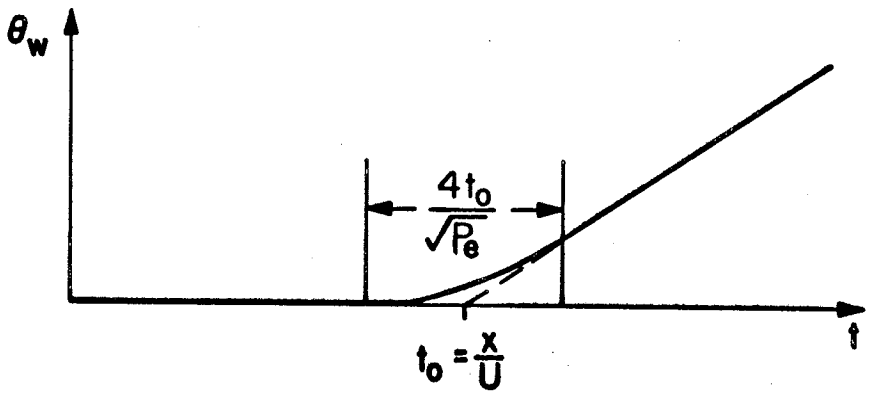

in the simple form $U = \ell/t_o$.

In practice, the determination of the level of the line $\theta_w = 0$ (the t-axis) on any physical display, such as an oscilloscope screen, is not always easy, nor is the determination of the slope always straightforward. In turbulent flows such determinations are impossible.

Returning to the analysis of equation (3), it is useful to normalize it to eliminate the effects of θ_1 and Nu. Note that $\theta(t) - \theta(t = x/U)$ is antisymmetric in time across the line $t = x/U$. Since $\theta(t = 0) = 0$, it follows that $\theta(t = 2x/U) = 2\theta(t = x/U)$. This is a reasonable measure of the amplitude of the temperature rise, which will be denoted by θ_m.* Hence

$$\theta_m = 2\,\frac{Nu\theta_1}{4}\sqrt{\frac{\pi}{Pe}}\,\exp\left[-\frac{Pe}{4}\,\frac{y^2}{x^2}\right]\,\mathrm{erf}\left[\frac{1}{2}\sqrt{Pe}\right]$$

and

$$\frac{\theta}{\theta_m} = \frac{1}{2}\left\{1 - \frac{\mathrm{erf}\left[\frac{1}{2}\sqrt{Pe}\left(1 - \frac{Ut}{x}\right)\right]}{\mathrm{erf}\left[\frac{1}{2}\sqrt{Pe}\right]}\right\}. \qquad (4)$$

The following values of θ/θ_m are evident:

(1) $\frac{\theta}{\theta_m}\,(t = 0) = 0$

(2) $\frac{\theta}{\theta_m}\,(t = \infty) \approx 1$

(3) $\frac{\theta}{\theta_m}\,(t = x/U) = \frac{1}{2}$.

* For reasonable values of Pe, the difference between $\theta(t = 2x/U)$ and $\theta(t = \infty)$ is less than 0.2%, which is well beyond the capabilities of the hot-wire temperature measuring system.

The third value of θ/θ_m suggests another method for finding U. The location of the half-amplitude point of θ is at the same point t_o discussed earlier, hence $U = \ell/t_o$. (See sketch of θ in Fig. 1.) It is important to note that the values of θ/θ_m at the three times $t = 0$, x/U, $2x/U$ are all independent of Pe, hence are invariant with changes in the gas properties.

In practice, for reasons to be discussed later, it is better to use the slope $\frac{d\theta}{dt}$ rather than θ. Since the maximum of $\frac{d\theta}{dt}$ occurs at $t = x/U$, the determination of the velocity is equally straightforward.

2.3 The Solution for Linear Temperature Rise

In the experiment under discussion the heat source is a fine wire heated by an electrical current pulse which rises with negligible rise time to a very high level and is shut off after a few microseconds. The wire temperature does not follow the current because of the thermal inertia of the wire, but rather has a behavior of the form

$$\theta_1 = \theta_p(1 - e^{-t/\tau_i}) \quad ,$$

where θ_p is the asymptote for θ_1 if the power were left on, and τ_i is the characteristic time constant of the wire, for this current level and fluid environment. If $t \ll \tau_i$, as is the case here, then $\theta_1 \approx \theta_p \frac{t}{\tau_i}$, a linear rise. When the current is shut off, at a time t_p, θ falls back to zero with a characteristic time constant $\tau_o \gg \tau_i$ since convection is

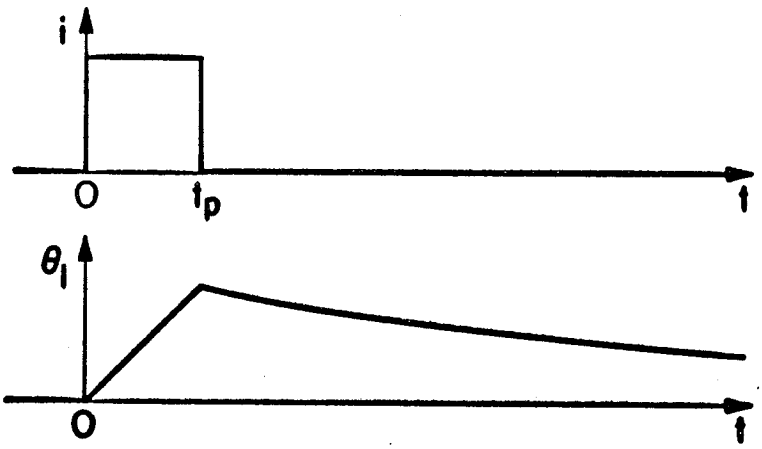

now the only influence on θ.

An analysis similar to that in sections 2.1 and 2.2 can be carried out in which the finite rise time of θ_1 is considered. Since τ_o is very large, the decay of θ is neglected, giving the assumed pulse shape shown by the broken lines on figure 2. The solution is obtained by a Duhamel integration of equation (2.4):

$$\theta(x, y, t) = \int_{t'=0}^{t'=t_o} \frac{d\theta_s(x, y, t - t')}{d\theta_1} d\theta_1(t')$$

$$= \int_{o}^{t_o} \frac{d\theta_s(x, y, t - t')}{d\theta_1} \frac{\theta_p}{t_p} dt' \quad ,$$

where θ_s is the solution in equation (2.4) for the step input. This gives the solution

$$\theta(x, y, t) = \frac{Nu\ \theta_p}{4}\sqrt{\frac{\pi}{Pe}}\ \exp\left[-\frac{Pe}{4}\frac{y^2}{x^2}\right]\Bigg\{\operatorname{erf}\left[\frac{1}{2}\sqrt{Pe}\right]$$

$$+ \frac{1 - \frac{tU}{x}}{\frac{t_p U}{x}}\ \operatorname{erf}\left[\frac{1}{2}\sqrt{Pe}\left(1 - \frac{tU}{x}\right)\right]$$

$$- \frac{1 - \frac{(t-t_p)U}{x}}{\frac{t_p U}{x}}\ \operatorname{erf}\left[\frac{1}{2}\sqrt{Pe}\left(1 - \frac{(t - t_p)U}{x}\right)\right]$$

$$+ \frac{2}{\sqrt{\pi Pe}}\frac{x}{t_p U}\left[\exp\left[-\frac{1}{4}\,Pe\left(1 - \frac{tU}{x}\right)^2\right]\right.$$

$$\left. - \exp\left[-\frac{1}{4}\,Pe\left(1 - \frac{(t - t_p)U}{x}\right)^2\right]\right]\Bigg\}\ . \qquad (5)$$

The point of symmetry in equation (5) can be found, for $t_p \ll \frac{x}{U}$, to be at $t = \frac{x}{U} + \frac{1}{2}\,t_p$, compared with $t = x/U$ for equation (4). Also, using the same approximation, for $\theta(t = \frac{1}{2}\,t_p) = 0$, hence it is seen that the time origin for velocity determination is at $t = \frac{1}{2}\,t_p$. A normalization of θ, using $\theta_m = \theta(t = 2\,\frac{x}{U} + \frac{1}{2}\,t_p) - \theta(t = \frac{1}{2}\,t_p)$ as the amplitude, and using the approximation $t_p \ll x/U$, gives

$$\frac{\theta}{\theta_m} = \frac{1}{2}\left\{1 + \frac{1 - \frac{tU}{x}}{\frac{t_p U}{x}} \frac{\operatorname{erf}\left[\frac{1}{2}\sqrt{Pe}\left(1 - \frac{tU}{x}\right)\right]}{\operatorname{erf}\left[\frac{1}{2}\sqrt{Pe}\right]}\right.$$

$$- \frac{1 - \frac{(t - t_p)U}{x}}{\frac{t_p U}{x}} \frac{\operatorname{erf}\left[\frac{1}{2}\sqrt{Pe}\left(1 - \frac{(t - t_p)U}{x}\right)\right]}{\operatorname{erf}\left[\frac{1}{2}\sqrt{Pe}\right]}$$

$$+ \frac{2}{\sqrt{\pi Pe}} \frac{x}{t_p U}\left[\frac{\exp\left[-\frac{1}{4} Pe \left(1 - \frac{tU}{x}\right)^2\right]}{\operatorname{erf}\left[\frac{1}{2}\sqrt{Pe}\right]}\right.$$

$$\left.\left. - \frac{\exp\left[-\frac{1}{4} Pe \left(1 - \frac{(t - t_p)U}{x}\right)^2\right]}{\operatorname{erf}\left[\frac{1}{2}\sqrt{Pe}\right]}\right]\right\} . \qquad (6)$$

This has the following significant values:

(1) $\frac{\theta}{\theta_m}\left(t = \frac{1}{2} t_p\right) = 0$

(2) $\frac{\theta}{\theta_m}\left(t = \infty\right) \approx 1$

(3) $\frac{\theta}{\theta_m}\left(t = \frac{x}{U} + \frac{1}{2} t_p\right) = \frac{1}{2}$

all of which are independent of Pe. Thus, except for the shift of all times by $\frac{1}{2} t_p$, the principle of velocity measurement remains unchanged. The behavior of θ (or $\frac{\theta}{\theta_m}$) and $\frac{d\theta}{dt}$ are sketched in figure 2 for no decay (dashed lines) and decay of the wire temperature (solid lines). The time

origin in figure 2 has been shifted by half the pulse width, so that $t_o = x/U$ is measured from the origin.

The temperature $\theta(t)$ at ℓ is sensed by a fine hot wire operated at a constant temperature greater than θ_m. The constant temperature operation allows the output signal to follow θ, except for a small shift due to the time constant of the hot wire circuitry.

2.4 Application of Turbulent Flows

In a turbulent flow the shape of θ is no longer the smooth curve of equations (4) or (7), but has wiggles in it caused by turbulent eddies of scale smaller than the wire spacing ℓ. For this reason the method of section 2.3 is no longer feasible for use on the turbulent signal.

If, however, the source wire is pulsed many times, a curve for $\theta(t)$* is obtained for each pulse. These curves can then be averaged together and, if sufficiently many pulses are used, a smooth curve $\overline{\theta}(t)$** is again obtained. From $\overline{\theta}(t)$, a transit time can be obtained as for the laminar flows. To distinguish this time from the laminar

---

* It is assumed from now on that all temperatures referred to are those at the sensing wire, i.e., $\theta(t) \equiv \theta(\ell, 0, t)$.

** The bar over a quantity such as θ denotes neither a time average nor a true stochastic average, but rather the time history of an "average" response. A particular point, say $\overline{\theta}(t_a)$ is obtained by averaging the values of the quantity θ at the time t_a after each pulse. Carrying out this process for all times gives the curve representing $\overline{\theta}(t)$. The same idea gives the fluctuation $\theta'(t) = \theta(t) - \overline{\theta}(t)$.

one, call it t_m, and call the one obtained from a single pulse (as in the laminar flow) t_o. Conceptually, at least, it is possible to measure a transit time for a single turbulent pulse which would correspond to an "instantaneous" velocity.* The relationship between t_o and U is the straightforward one $U = \ell/t_o$. If the flow is turbulent, large eddies with a scale larger than ℓ will cause the θ curve to readjust to the velocity in the eddy, while small eddies (scale $< \ell$) have their main effect in adding random fluctuations to the profile. These small random fluctuations have so far defied any attempts at meaningful analysis of their effect on the averaged pulse shape, but probably do not average to zero because of the non-linear relation between velocity fluctuations and temperature fluctuations.

In the following discussion a method is presented for determination of the velocity fluctuations due to the large eddies. If ℓ is small enough, compared to the scale of the turbulence, then most of the turbulence can be accounted for by the probe.

It is convenient here to introduce a slightly different notation. Let $\theta(t, U)$ be the profile of temperature at $x = \ell$ for a laminar flow at velocity U. Define the time t_o

---

* "Instantaneous" is in quotation marks because the velocity measured is actually an average velocity over the duration of a trip from the heat source to the sensing wire. The probe measures transit times, not velocities.

by $\frac{\partial^2\theta}{\partial t^2}(t_o, U) = 0$. This time corresponds to the time at the half-amplitude point in the θ profiles as previously discussed, so $U = \ell/t_o$. Let $U = \overline{U} + u$, where $\overline{U}$ is the mean velocity and u is a fluctuation due to a large eddy, and write $\theta(t, U)$ in a Taylor series in u. Assuming a normal distribution for u,and θ-profiles such as those in equations (3) and (5), it can be shown that

$$\overline{\theta(t, U)} = \theta(t, \overline{U}) + \frac{1}{2} t^2 \frac{\partial^2\theta}{\partial t^2}(t, \overline{U}) \frac{\overline{u^2}}{\overline{U}^2} + \frac{1}{8} t^4 \frac{\partial^4\theta}{\partial t^4}(t, \overline{U}) \left(\frac{\overline{u^2}}{\overline{U}^2}\right)^2 + \ldots \quad (7)$$

and

$$\overline{[\theta'(t, U)]^2} = \left[t \frac{\partial\theta}{\partial t}(t, \overline{U})\right]^2 \frac{\overline{u^2}}{\overline{U}^2} + \frac{1}{2} t^4 \frac{\partial\theta}{\partial t}(t, \overline{U}) \frac{\partial^3\theta}{\partial t^3}(t, \overline{U}) \left(\frac{\overline{u^2}}{\overline{U}^2}\right)^2 + \ldots \quad (8)$$

The details of the derivation of equations (7) and (8) are contained in Appendix A.

At $t = t_o$, where $\frac{\partial^2\theta}{\partial t^2} = \frac{\partial^4\theta}{\partial t^4} = 0$, equation (7) shows that $\overline{\theta(t_o, U)} = \theta(t_o, \overline{U})$, so the mean profile and a single profile for velocity $\overline{U}$ cross at t_o (as sketched in Fig.3). However, t_o is not the point of maximum slope for $\overline{\theta}$ since differentiation of equation (7) gives

$$\frac{\partial^2\overline{\theta}}{\partial t^2}(t_o, U) = 2\, t_o \frac{\partial^3\theta}{\partial t^3}(t_o, \overline{U})\, \frac{\overline{u^2}}{\overline{U}^2} + \ldots \quad , \quad (9)$$

which is a negative number. So, the measured delay from the mean profile, t_m, defined by $\frac{\partial^2\overline{\theta}}{\partial t^2}(t_m, U) = 0$, will not be the same as t_o.

Equations (7) and (9) lead to the profiles and their slopes which are sketched in figure 3.

To determine the mean velocity, $\overline{U}$, it is necessary to calculate the relationship between t_m and t_o, which, in turn, requires a relation between $\overline{u^2}/\overline{U}^2$ and $\overline{\theta'^2}(t_m, U)$. The required relations, calculated in Appendix A, are

$$t_o = t_m \left(1 + \frac{2\,\frac{\overline{u^2}}{\overline{U}^2}}{1+\frac{\overline{u^2}}{\overline{U}^2}} \right) + O\left(\frac{\overline{u^2}}{\overline{U}^2}\right)^3 \quad (10)$$

and

$$\frac{\overline{u^2}}{\overline{U}^2} = \frac{\overline{\theta'^2}\,(t_m, U)}{t_m^2 \left[\frac{\partial\overline{\theta}}{\partial t}(t_m, U)\right]^2} + O\left(\frac{\overline{u^2}}{\overline{U}^2}\right)^3 \quad . \quad (11)$$

Equations (10) and (11) complete the set of equations required to determine the mean velocity and the mean-square fluctuation level about that mean. The fluctuation level is obtained directly from equation (11) in terms of the maximum slope of the mean profile, $\frac{\partial\overline{\theta}}{\partial t}$, the time at which the maximum occurs, t_m, and the mean-square fluctuations

of the signal voltage at t_m, $\overline{\theta'^2}$. The transit time, t_o, can then be calculated by using equation (10), and the mean velocity follows easily from

$$\overline{U} = \frac{\ell}{t_o} \quad . \tag{12}$$

III. DESCRIPTION OF THE APPARATUS

Experimental data were obtained for the flow of a gas issuing from a circular nozzle into a reservoir containing either the same or a different gas. The velocity fields for several combinations of gases were mapped using a probe operating according to the principles of section II.

3.1 The Jet

The physical layout of the jet is shown in figure 4. The incoming gas is filtered and its pressure is regulated to any desired value less than 60 psig. It flows through a fast-acting solenoid valve, which opens to start the experiment, and then through a sonic needle valve which controls the flow rate. The flow rate is measured by a hot wire in the jet which enters the settling tube. At the other end of the settling tube is a circular nozzle of 1/8" to 1/2" diameter mounted in a 5"- diameter flat endplate. The exit of the nozzle is sealed between runs by a shutter-line vane which is moved out of the way by a solenoid when the pressure in the settling tube slightly exceeds the reservoir pressure.

The settling tube is mounted through the top of the reservoir and is adjustable in position vertically. The reservoir is completely sealed, so the gas in it can be at any pressure from about 1 mm Hg to 4 atmospheres. A vacuum pump can pump out the gas in the tank, which can then be

filled with any desired reservoir gas. A set of electrically actuated venting valves keeps the reservoir pressure approximately constant ($\pm$ 1%) during a run. Observation windows on the tank enable shadow photography of the flow.

The vane covering the nozzle is necessary because of a very limited running time (Sec. 3.3). If there is no vane, the settling tube is filled with the reservoir gas before a run, since the nozzle connects the two regions. When the solenoid valve is opened to start the flow, a jet of the jet gas enters the settling tube and a mixture flows out of the nozzle. The flow rates are usually sufficiently low that it takes a long time to purge the settling tube completely. This mixture contaminates the reservoir gas and severely shortens the already short flow times. On the other hand, with the vane, the settling tube can be sealed off from the reservoir, enabling it to be filled with the jet gas before a run. Yet the vane does not alter the nozzle and settling tube geometry during a run (as would be the case with any ordinary valve in that region of the apparatus). The vane is seated against an O-ring in the nozzle block by a small positive pressure differential of the reservoir pressure over that in the settling tube. The solenoid which moves the vane out of the way is unable to operate until this pressure differential is relieved by allowing gas to begin flowing into the settling tube.

Instrumentation in the reservoir consists of a pitot tube, a hot wire off to the side of the nozzle outlet which monitors the composition of the reservoir gas, and a pneumatically driven traverse on which can be mounted a hot wire probe, a pitot tube, or the probe described in section 3.2. A linear potentiometer connected to the traverse monitors the position of the traverse with an accuracy better than 0.001".

There are multiple pressure ports and BNC-type sealed electrical connectors in the walls of the tank and settling tube to enable control and monitoring of the experiment.

3.2 The Heat Pulse Velocity Probe

The physical construction of the probe is shown in figure 5. The heat source is a wire of an alloy composed of 84% platinum, 10% rhodium, and 6% ruthenium* and is 0.0004" in diameter and 0.2" long. Originally a standard hot wire alloy (90% Pt, 10% Rh) was tried, but was found unsatisfactory for several reasons, viz., too low tensile strength, too low resistance, and too high thermal coefficient of resistance. The low tensile strength meant that the wire, which is subjected to continuous thermal stresses, had a very short lifetime. The low resistance did not allow efficient use of the power available from a Hewlett Packard 214A Pulse Generator. The output impedance of the 214A is

* Obtained from the Sigmund Cohn Corp., Mt. Vernon, N.Y.: alloy #851.

50 ohms, which was well above the wire resistance. The high thermal coefficient of resistance meant that the resistance of the wire nearby doubled during the heating process, which again gave impedance matching problems with the pulse generator. The low tensile strength required a large wire which, in turn, had a low resistance but required large amounts of power to heat rapidly and which cooled slowly, requiring long intervals between successive pulses. The overheat obtainable using the maximum power consistent with reasonable wire life, for a 0.0005" diameter wire, was about 50^{o} C.

Tungsten meets the requirement of high strength, but oxidation at high temperatures makes the lifetime very short. The Pt-Rh-Ru alloy is about four times as strong as the Pt-Rh alloy, has nearly twice the resistance, and has a thermal resistance coefficient which is one third as large. To reduce the required power and the cooling time, the diameter was reduced to 0.0004", which still gives adequate strength and further increases the wire resistance. The resistance of the wire on the probe is about 30 ohms at room temperature. Applying the full power output from the 214A pulse generator for 5 μs (about 70 volts at 2 amperes) heats up the wire by about 350^{o} C, increasing the resistance to about 40 ohms.

The expansion and contraction of the wire upon heating and cooling eventually causes failure due to fatigue at the

points where the wire is soldered to the supporting needles. It was found possible to extend the lifetime of the wire considerably by mounting the wire through small watch jewels ($\sim$ 0.01" dia., with a 0.003" hole) and then soldering it, in slight tension, to the sides of the needles (see detail, Fig. 5). The jewels allow the wire to slide back and forth as it expands and contracts, with no points of stress concentration. The slight tension assures that the wire remains sufficiently tight so that it is not bowed by the flow. The lifetimes of wires mounted this way are nearly infinite if properly installed and properly operated.

There are four sensing wires mounted perpendicular to the source wire and about 0.06" downstream of it. The wires are spaced on 0.04" centers, enabling measurement of the velocity at four points simultaneously.

Bauer (Refs. 9 and 10) mounted his sensing wire parallel to the source wire. By adjusting the relative positions of the two wires until the output was a maximum, he could determine the flow direction. In a short duration flow such a technique is not applicable, hence it was important that data be obtained even if the probe axis was slightly misaligned with the flow direction. With the crossed axes of the two wires it is possible to accomplish this. The width of the wake of the source wire has been found experimentally to be in the range 0.010" to 0.015", depending on the flow conditions at the sensing wire position, which

All the wires on the probe are mounted on needles made of #80 drill rod (0.013" dia.) which was tapered to about 0.006" diameter by etching in acid.

3.3 The Instrumentation

As was mentioned in section 3.1, there are hot wires in the settling tube and in the tank near the jet orifice (2½" from the jet centerline and ¼" below the plane of the orifice). These wires, both of which are connected to constant temperature hot wire circuitry, monitor respectively the flow rate of the jet gas and the composition (i.e., the thermal conductivity) of the reservoir gas near the jet. The monitoring of the gas composition is necessary since the reservoir is sealed, except for vents to maintain the pressure constant, and hence the reservoir gas becomes contaminated by the jet gas. The gas-composition-monitoring hot wire detects the presence of jet gas in the recirculating flow which is set up in the tank by the jet. Under typical conditions the gas-composition-monitoring hot wire detects the first appearance of the jet gas about 2 to 3 seconds after the flow begins, with significant proportions present about one second later.

The traverse in the tank is driven by a Bellofram piston which is operated by compressed air. The piston is an extremely low friction device which was originally installed to allow rapid hot wire surveys of the flow field

without exposure to the electrical noise generated by electric motors. It enables smooth traverses of about two inches of the flow field in times as short as 0.1 seconds. Although it was not used for this purpose in this experiment, it provided a satisfactory method of positioning the probe for each run.

The traverse is connected to a linear potentiometer with a fixed voltage applied to it. The output from the potentiometer is displayed by a digital voltmeter for easy determination of the probe position.

The sensing wires on the heat pulse velocity probe are each connected to a Miller M-5 constant temperature hot wire amplifier which was slightly modified to accept higher resistance wires. The wires are operated at very low overheat with heating currents of less than 1 mA.

The output from the hot wire units is amplified about 600 times by A-C coupled wide-band amplifiers and the amplified signals are recorded on magnetic tape.

The heart of the instrumentation is a Consolidated Electrodynamics VR-3400 magnetic tape recorder which can record 14 channels of data on 1" wide magnetic tape at tape speeds from 3 3/4 to 120 inches per second (ips). The signals from the four sensor wires were recorded through FM electronics (frequency band 0 to 40 kHz) on tracks 1 through 4 of the tape at a tape speed of 120 inches per second. The signals from the flow and gas-composition hot wires were

recorded (also FM) on tracks 5 and 6. (Table 1 summarizes the data recorded on each track.)

The recorder generates a square wave signal (a "clock signal") at a frequency proportional to the set tape speed (200 kHz at 120 ips) which is recorded, through direct record electronics, on track 8. This signal serves several purposes which will be mentioned below.

A signal proportional to the current pulses applied to the heat source wire is recorded, again through direct recording, on track 9. Tracks 10 through 14 are unused. The FM signal which is recorded on track 7 will be discussed in the next section.

In addition to being recorded on track 8, the 200 kHz clock signal from the recorder is also fed into a Beckman 6014A Preset Reversing Accumulator. This instrument counts cycles of the clock signal and, upon reaching a preset number, provides a trigger pulse which is used to trigger the pulse generator which heats the source wire. The preset counter then resets itself and repeats the procedure. Since the heating pulse spacing is usally 4 or 5 ms, this means that the Beckman counter provided a trigger for every 800 or 1000 cycles of the 200 kHz clock signal.

Additional instruments are a micromanometer for use with the pitot tubes, a cathetometer which is used for initial positioning of the probe, and a Tektronix 555 dual beam oscilloscope which became intimately involved in the

control of the experiment, as will be discussed in the next section.

3.4 The Control Circuitry

A reasonably elaborate system of electrical controls was necessary to operate the experiment to conserve both expensive gases and magnetic tape. The recording was performed at a tape speed of 120 inches per second, at which rate a few extra seconds of recording per run for the approximately 550 runs would consume enormous quantities of tape. This extra useless tape would also have increased the time required for data reduction at the reduced playback speeds necessary for the data reduction process (see section 6.1). So, the delays inherent in manual coordination of the operations of the experiment and the tape recorder were unacceptable.

The control circuitry coordinates the operation of the jet and the tape recorder by using signals from the internal control circuitry of the recorder as well as the two time bases of a Tektronix 555 oscilloscope. The entire run takes place automatically upon pressing the start button of the tape recorder. When the recorder has accelerated to full speed (about 6 seconds and 28 feet of tape after starting) it provides a signal which lights a lamp on its panel. This signal, tapped from one of the circuit boards in the recorder, was used to trigger the sweep in time base A of the

oscilloscope. The sweep rate n is set to be 1/10 the desired flow duration, so that the sweep of the 10 cm wide scope face takes 10n seconds. During these 10n seconds the oscilloscope provides a low impedance +20 volt gate signal which is used to operate a relay which, in turn, switches on the power to the various solenoid valves controlling the flow. This gate signal is also attenuated (by a factor of about 10) and the attenuated signal is recorded on track 7 of the recording tape.

The trigger to time base A also triggers a delay generator in the oscilloscope. The delay generated can be set to any multiple m of the sweep rate n, at the end of which a trigger pulse, delayed by m x n seconds from the first trigger pulse, is generated. This pulse triggers time base B which immediately provides a +20 volt gate signal for 50 milliseconds. This gate signal momentarily energizes a relay which opens the circuit between two terminals of a remote control connector on the recorder. The momentary opening of this circuit releases an internal relay which shuts off the tape transport (which then comes to a stop in about 4 seconds and 15 feet of tape).

Thus, the controls can be set to provide a flow running time of 10n seconds, during m x n of which recording is taking place. The running time is typically between 1 and 5 seconds, so n ranges from 0.1 to 0.5 seconds. Usually m is 10. A positive signal is recorded on track 7 of the

tape during the run, thus the duration of the recording run is also marked on the tape.

IV. THE EXPERIMENTAL PROCEDURE

The procedures involved in recording data varied depending on the experiment being performed. These can be divided into three categories: (1) probe calibrations; (2) runs in homogeneous flows, where the jet gas and reservoir gas are the same; and (3) runs in inhomogeneous flows.

4.1 Probe Calibration

Calibrations of the probe were performed with the probe and a pitot tube inserted in the core region of a ½" diameter jet. The tank vents were left fully open and the flow was run, under manual control, sufficiently long to read a fluid micromanometer connected to the pitot tube and to record one second of data. The flow in the vicinity of the probe and pitot tube, which are usually 1/8" downstream of the orifice near the jet centerline, is sufficiently uniform that all the probe wires and the pitot tube are exposed to the same velocity. The control circuitry operates the tape recorder but is disconnected from the flow controls.

A few calibration runs were made in which only one sensing wire of the probe was used in the normal manner. The overheat on an adjacent wire was increased sufficiently so that it operated as a normal hot wire. The signal from this second wire was linearized and connected to a RMS voltmeter. This probe was then placed in several turbulent

flows in jets and in the Kármán vortex street behind a circular cylinder to subject it to high velocity fluctuation levels. These runs constituted a check for the data reduction method which computed the turbulence intensity.

Playback of some of the calibration recordings revealed that the tape recorder electronics had added a ringing signal to the start of each pulse response. The apparent cause was overdriving of the record amplifiers by a very large spike of short duration, the source of which was probably electromagnetic coupling of the heating current pulse with the sensing wire and circuit. This ringing signal was recorded alone, with no flow present, so that later processing could eliminate it from the temperature trace.

4.2 Homogeneous Flows

Runs in which the jet gas and reservoir gas were the same (i.e., air) were handled much the same as the probe calibrations, except the pitot tube was no longer present. Because of limitations on the travel of the settling tube, and to keep all measured velocities sufficiently large to allow for easy processing, a complete survey required the use of three nozzles which were somewhat similar geometrically, but not completely so. The region between $x/d = 0.5$ and $x/d = 12$* was surveyed using a ½" diameter nozzle; that between $x/d = 4$ and $x/d = 16$ with a 3/8" diameter nozzle;

---

* See figure 6 for definitions of coordinates.

between x/d = 8 and x/d = 24 with a ¼" diameter; and between x/d = 12 and x/d = 48 with a 1/8" nozzle. The Reynolds numbers $Re_d = \frac{U_o d}{\nu}$ were 1.5 x 10^4 for the flows with the various nozzles, meaning that the nozzle velocities were the largest on the small nozzles, for which the surveys were farthest downstream.*

At each axial position the flow was surveyed radially from a point slightly off the jet centerline to a point on the other side of the centerline where the flow was highly oblique to the axis, as indicated by a very high intermittency of the sensor signals observed on an oscilloscope. The radial point spacing was always equal to or less than 0.04" (the spacing between adjacent sensor wires). Recording times ranged from one to five seconds, with the longer recording times for the more turbulent regions.

4.3 Inhomogeneous Flows

Three different cases were surveyed in which the jet gas was different than the ambient gas: (a) helium (molecular weight M = 4) flowing into air ("molecular weight"= 28.97); (b) air flowing into helium; and (c) helium flowing into sulfur hexafluoride, SF_6 (M = 146). These gave the

---

* The use of such a sequence of nozzles is of some importance for the inhomogeneous case because it minimizes the significance of the buoyancy.

ratios of jet gas density to reservoir gas density of 7.24, 0.138, and 0.027 respectively. Each case required slightly different handling.

Shadow photographs such as those in figure 7 show the basic characteristics of inhomogeneous jets. The nozzle boundary layer becomes unstable soon after leaving the nozzle. The instability develops into vortex rings which eventually break down into turbulence. This pattern is particularly evident in figure 7 for the air-He case at Re_d = 14,000. For very high Re_d the nozzle boundary layer may be turbulent, as in the air-He photograph for Re_d = 30,000, but the scale of the breakdown process in the shear layer is sufficiently larger than the scale of the boundary layer turbulence, so that the shear layer breakdown is still visible.

Each shadow photograph shows a point downstream of the nozzle where the reasonably regular vortex-ring structure of the shear layer has broken down into the irregular pattern which is characteristic of turbulence. The location of this point is more easily determined for some flows than for others, and at best any such measurement is more qualitative than quantitative, but it does give some measure of the length of that portion of the flow which is most greatly influenced by the nozzle geometry and conditions.

A comparison of these development lengths showed that they were approximately the same for different gas combina-

tions if the jet Reynolds numbers were scaled as the square root of the jet/ambient density ratio. It seemed reasonable to choose flow conditions such that these distances were the same for various flows. Choosing $Re_d = 1.5 \times 10^4$ for the air-air case gives then $Re_d \approx 5500$ for He-air, $Re_d \approx 4 \times 10^4$ for air-He, and $Re_d \approx 2500$ for He-SF_6.

These conditions could easily be achieved, with one exception. The required velocities in the air-He case were so large that the measured heat pulse transit times were extremely small. In addition, the resulting dynamic pressures on the probe were so great that the relatively long heat source wire was bowed toward the sensing wires, thereby altering the wire spacing. To reduce the dynamic pressures and to increase the delays, the reservoir was pressurized to a pressure of 3 atmospheres. This divided the velocity by a factor of three, divided the dynamic pressure by three and multiplied the transit times by three.

The He-air runs were made with all tank vents open. In the other cases they were opened sufficiently by the control circuitry to maintain approximately constant reservoir pressure. The shutter valve was used in all cases.

For a run the sequence of events was similar for any of the three gas combinations. The probe and settling tube were positioned and the reservoir was pumped out and filled to the appropriate pressure with the desired gas. The settling tube was filled with the jet gas. The start button

on the tape transport was pressed, causing it to accelerate to full speed, the jet and vent solenoid valves to open, and the shutter valve to open slightly later. The control circuitry closed off all valves and stopped the recorder after preset lengths of time (1 to 5 seconds). The signals from the flow and concentration sensors and the pulser were photographed on an oscilloscope screen, as well as being recorded, enabling instant verification that everything operated properly. The contamination level in the reservoir was checked using the composition sensing wire and, if it exceeded a level corresponding to a 1% change in reservoir density, then the reservoir was pumped out and refilled. Otherwise the same gas was used. The next run then followed the same pattern.

V. THE DATA REDUCTION PROCESS

5.1 Analog to Digital Conversion

The entire experiment yielded data stored on eleven 3600' reels of magnetic tape. For computer processing this data had to be selectively sampled and converted to digital form by an analog-to-digital converter. The signal is played back by the tape recorder and is sampled at selected points by the converter, which then converts it to digital form and feeds it to an IBM 7040 computer which writes the digitized data on another magnetic tape. The converter is able to sample a voltage in less than a microsecond, but is not able to sample again until slightly over 100 microseconds have elapsed. This sampling rate of somewhat less than 10 kHz caused some difficulty.

The pulse transit times encountered in the experiment range from 500 to 2000 μs. To effectively resolve the shorter times ($t_m \lesssim 250$ μs) sampling every 5 μs was desired, while 10 μs was an adequate spacing for the longer times corresponding to lower velocities. But, sampling at 200 kHz (corresponding to 5 μs spacing) was impossible with a 10 kHz converter, unless the data rate could be scaled in some way. The tape recorder itself accomplished this. By recording at 120 ips and playback at 3 3/4 ips, all times were scaled by a factor of 32. This meant that points 5 μs apart during recording were 160 μs apart during playback,

well within the capabilities of the converter.

Fortuitously, the servo signal generated by the tape recorder (discussed in section 3.3) had a frequency of 200 kHz at the 120 ips recording speed, thus it provided a convenient clock signal for the digitization process if recorded on the tape at the same time as the data. Hence, each pulse of the clock signal initiated the sampling of a data point on playback. For the 10 μs point spacing, every other pulse was used. Since the sampling rate was now half as great, tape playback could be at a speed of 7½ ips to conserve time.

Each of the four data tracks was digitized individually. Since 3600 feet of tape requires 192 minutes for playback at 3 3/4 ips, any steps to speed up the process were welcomed. In addition to making use of the faster 7½ ips whenever possible, the signals on channels 5, 6 and 7 were used to restrict the sampling to usable portions of the signal, with the tape being run at high speeds through unusable sections.

The sampling could begin when the gate signal appeared on track 7. The actual sampling for each pulse was started by a trigger signal from the pulser signals on track 9 of the tape, and was then controlled at a rate determined by the clock signal from track 8. The number of pulses to be sampled in a run was preset (corresponding to the contamination-free time determined by the gas composition sensor data

on track 6), as was the number of samples per pulse. In addition a certain number of pulses at the start of each run were ignored. These pulses occurred during the starting-up time of the flow. The exact number to be ignored was determined by the data from the flow sensor on track 5. (Usual start-up times were ~ 60 ms.) Sampling was terminated when the preset number of pulses was exceeded or when the gate signal on track 7 disappeared (signifying the end of the recording for that run).

During the recording of each run (or during later playback of the tape) each probe signal was observed on an oscilloscope and the duration between the source heat pulse and the peak of the sensor response was noted. During the analog-to-digital conversion, only the portion of each signal during this time interval was sampled. The remainder of the recorded signal between these portions was not sampled.

This entire process resulted in 9×10^7 samples of digitized data which were stored on 15 reels of computer tape for further processing.

5.2 The Relation Between the Temperature and the Sensor Signal

In order to calculate the flow velocity according to the method of part II, it is necessary to relate the digitized voltages to the temperature profiles. The voltage

output, v, from a hot wire operated at constant temperature, T,* can be expressed by King's law as $v^2 = (T - \theta)(A + B\sqrt{Pe})$. Here θ is the temperature of the gas flowing over the wire and Pe is the Peclet number, $Pe = Pr \times Re_d$. When $\theta = 0$ let $v = v_o = [T_w(A + B\sqrt{Pe})]^{\frac{1}{2}}$ and express v as $v = v_o + v_{Pe\theta}$. The variable $v_{Pe\theta}$ is the voltage change caused by presence of a flow or a heat pulse, or both. From the above, it can be found that

$$\theta = - \frac{v_{Pe\theta}(v_{Pe\theta} + 2v_o)}{A + B\sqrt{Pe}} \qquad (13)$$

or

$$v_{Pe\theta} = - v_o + [(T_w - \theta)(A + B\sqrt{Pe})]^{\frac{1}{2}}. \qquad (14)$$

There are not particularly convenient relations to work with. For low overheat of the sensing wire under the experimental conditions discussed earlier, $|v_{Pe\theta}| < 4mV$ while $v_o > 40$ mV so it seems reasonable to neglect $v_{Pe\theta}$ as compared to $2v_o$ in equation (13). This gives the simpler relation

$$\theta = - \frac{2v_o}{A + B\sqrt{Pe}} v_{Pe\theta} \quad , \qquad (15)$$

which says that θ is essentially proportional to $- v_{Pe\theta}$ during any particular run during which $\sqrt{Pe}$ does not vary greatly.

A plot of equation (13) or (14) looks like

---

* It is assumed that $T > \theta$ at all times.

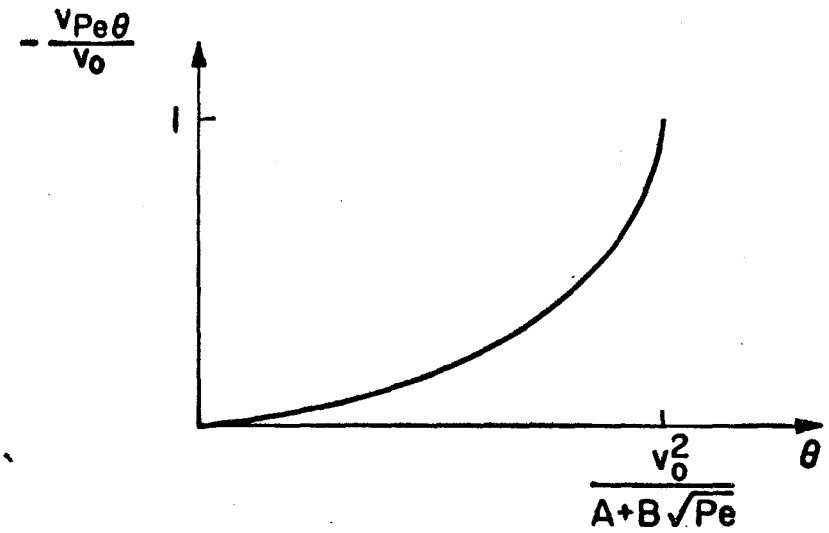

The linear variation of $v_{Pe\theta}$ with θ near the origin is apparent. It can be seen that $|\frac{v_{Pe\theta}}{v_o}| << 1$ does not imply $\theta << \frac{v_o^2}{A + B\sqrt{Pe}}$, although the converse does hold. The less restrictive assumption $|\frac{v_{Pe\theta}}{v_o}| << 1$ is sufficient.

If now $\theta = \overline{\theta} + \theta'$ and $Pe = \overline{Pe} + Pe'$, substitution into equation (14) and expansion of the radical for $|\theta'| << T - \overline{\theta}$ and $|Pe'| << Pe$ gives

$$v_{Pe\theta} = - v_o + \left[(T - \overline{\theta})(A + B\sqrt{\overline{Pe}})\right]^{\frac{1}{2}} \cdot \left\{1 - \frac{1}{2}\frac{\theta'}{T - \overline{\theta}} + \frac{1}{4}\frac{B\sqrt{\overline{Pe}}}{A + B\sqrt{\overline{Pe}}}\frac{Pe'}{\overline{Pe}} + \ldots\right\}. \quad (16)$$

Thus

$$\overline{v}_{Pe\theta} = - v_o + \left[(T - \overline{\theta})(A + B\sqrt{\overline{Pe}})\right]^{\frac{1}{2}}$$

implying

$$\overline{\theta} = - \frac{\overline{v}_{Pe\theta}(\overline{v}_{Pe\theta} + 2v_o)}{A + B\sqrt{\overline{Pe}}} \quad (17)$$

if the second degree fluctuating terms are neglected. These

are the turbulent mean equivalents of the laminar flow equations (13) and (14).

Also from equation (16), the fluctuating part is

$$v'_{Pe\theta} = \left[(T - \bar{\theta})(A + B\sqrt{\overline{Pe}})\right]^{\frac{1}{2}} \left\{ -\frac{1}{2}\frac{\theta'}{T-\bar{\theta}} + \frac{1}{4}\frac{B\sqrt{\overline{Pe}}}{A+B\sqrt{\overline{Pe}}}\frac{Pe'}{\overline{Pe}} \right\}.$$

This invites an obvious separation $v'_{Pe\theta} = v'_{Pe} + v'_{o}$, where v'_{Pe} is the fluctuation due to changes in the flow velocity or properties and v'_{θ} is the primary change due to the heat pulse. Some manipulation then yields

$$\overline{v'^2_{Pe}} = \frac{1}{16}\frac{B^2}{\overline{Pe}}\left[\frac{v_o + \bar{v}_{Pe\theta}}{A + B\sqrt{\overline{Pe}}}\right]^2 \overline{Pe'^2} \qquad (18)$$

and

$$\overline{v'^2_{\theta}} = \frac{1}{4}\left[\frac{A + B\sqrt{\overline{Pe}}}{v_o + \bar{v}_{Pe\theta}}\right]^2 \overline{\theta'^2} \quad . \qquad (19)$$

Using the fact that $\bar{v}_{Pe\theta} \ll v_o$ simplifies equations (17), (18), and (19) to

$$\bar{\theta} = -\frac{2v_o}{A + B\sqrt{\overline{Pe}}}\bar{v}_{Pe\theta}$$

$$\overline{v'^2_{Pe}} = \frac{1}{16}\frac{B^2}{\overline{Pe}}\left[\frac{v_o}{A + B\sqrt{\overline{Pe}}}\right]^2 \overline{Pe'^2} \qquad (20)$$

$$\overline{v'^2_{\theta}} = \frac{1}{4}\left[\frac{A + B\sqrt{\overline{Pe}}}{v_o}\right]^2 \overline{\theta'^2} \qquad (21)$$

A significant relation is obtained by dividing equation (21) by the square of equation (17):

$$\frac{\overline{v_\theta'^2}}{\overline{v}_{Pe\theta}^{\,2}} = \frac{\overline{\theta'^2}}{\bar{\theta}^2} \tag{22}$$

This allows voltages to replace temperatures in equation (11).

These relations combine with equations (10), (11), and (12) to give all the formulas required for computing the flow mean velocity and turbulence level:

$$\overline{U} = \frac{\ell}{t_m} \frac{1 + \dfrac{\overline{u'^2}}{\overline{U}^2}}{1 + 3\dfrac{\overline{u'^2}}{\overline{U}^2}}$$

where

$$\frac{\overline{u^2}}{\overline{U}^2} = \frac{\overline{v_\theta'^2}\,(t_m)}{\left[t_m \dfrac{d\overline{v}_{Pe\theta}}{dt}\,(t_m)\right]^2} \cdot \tag{24}$$

5.3 The Real Signal Versus the Idealized One

By the time the sensor signal has been amplified, recorded and played back for conversion, it has changed form somewhat from the ideal signal discussed in the preceding section. This section discusses how the data was processed in order to extract as true a temperature profile as possible.

First, it is obvious that the discussion of part II is overly idealized. In reality the heat source and sensing wires are of finite size with boundary layers, hence the solutions of section 2.3 can be considered only as approximations. In actuality the heat pulses are more diffused because of the boundary layer effects and are not of the antisymmetric error function form because of the cooling of the source wire when the pulse ends. The latter effect causes a pulse with a rounded peak, as shown in figure 2.

As can be seen in figure 8, the recording electronics has introduced a ringing signal at the beginning of the trace. (The steps in the levels of the data points in figure 8 indicate the resolution of the computer printer, not of the digitization.) Further, the AC-coupled amplifier has introduced an artificial zero level to the signal. Additionally, all electronic devices introduce noise. Although this noise should average to zero for the mean pulse shape, it will have an effect on the turbulence calculation.

There is one additional form of "noise" which is more

troublesome. The sensing wires, being slightly heated electrically, respond in standard hot wire fashion to the velocity and density of the stream. Any shift due to a laminar flow disappears in the AC-coupled circuitry, but a fluctuating signal from a turbulent stream remains. This again averages to zero for the mean signal, but causes problems in the turbulence calculations.

Assume that the signal which is digitized, v, can be written as a superposition of the desired signal, v_θ, and all of the unwanted extra effects:

$$v = v_\theta + v_r + v_n + v_z + v_{Pe}$$

where v_r is the ringing, v_n is the noise, v_z is the zero shift and v_{Pe} is the "hot wire effect". Each term can be decomposed into a mean value and a fluctuating term, e.g., $v_r = \overline{v_r} + v_r'$. Some simplifications occur immediately. The mean of the noise should be zero, $\overline{v_n} = 0$. The magnitude of the mean zero level shift $\overline{v_z}$ (corresponding to $-v_o$ in section 5.2) is unimportant if $|v_z| \ll |v_{max}|$, as discussed in section 5.2, so set $\overline{v_z} = 0$. Similarly one can set $\overline{v_{Pe}} = 0$. The terms v_r' and v_z' need some explanation. The $v_r'(t)$ gives the deviation of the ringing, during any particular pulse, from a mean ringing signal. A cause for such a fluctuation could be different signal levels at different pulses, for example. Similarly, changes in the signal from one pulse to the next cause small changes in the zero level

set by the AC-coupled amplifier, causing v_z' .

The averaging then gives

$$\bar{v}_\theta = \bar{v} - \bar{v}_r$$

and

$$v_\theta' = v' - (v_r' + v_n' + v_z' + v_{Pe}') \ .$$

Noting that $\overline{v_{Pe}' v_r'} = \overline{v_{Pe}' v_n'} = \overline{v_{Pe}' v_\theta'} = 0$, the mean square voltage fluctuation becomes

$$\overline{v_\theta'^2} = \overline{v'^2} - \overline{v_z'^2} - \overline{(v_n' + v_r')^2} - \overline{v_{Pe}'^2} \ . \qquad (25)$$

Now consider a case where there is no flow but everything else is as before. Denote signals for this case with the subscript $(\ )_o$. Then $\bar{v}_{\theta_o} = \bar{v}_o - \bar{v}_{r_o}$. But v_{θ_o} should be zero, since there is no flow convecting the heat to the sensing wire. Hence $\bar{v}_o = \bar{v}_{r_o}$.

It seems reasonable to assume that the ringing is independent of the flow, hence $\bar{v}_r = \bar{v}_{r_o} = \bar{v}_o$.

Similarly $v_{\theta_o}' = v_o' - (v_{r_o}' + v_{n_o}' + v_{z_o}' + v_{Pe_o}')$. Here v_{θ_o}' should be zero, as should v_{Pe_o}' (since there is no velocity). The noise should not depend on the flow (at least to any great extent) so assume $\overline{v_{n_o}'^2} = \overline{v_n'^2}$ as well as $\overline{v_{r_o}'^2} = \overline{v_r'^2}$.

Then

$$\overline{v_{\theta_o}'^2} = 0 = \overline{v_o'^2} - \overline{v_{z_o}'^2} - \overline{(v_{n_o}' + v_{r_o}')^2}$$

and, using $\overline{(v'_{n_o} + v'_{r_o})^2} = \overline{(v'_n + v'_r)^2}$ since $\overline{v'_{n_o} v'_{r_o}} = 0$, gives $\overline{(v'_n + v'_r)^2} = \overline{v'^2_o} - \overline{v'^2_{z_o}}$. Substituting this into equation (25) gives

$$\overline{v'^2_\theta} = \overline{v'^2} - \overline{v'^2_z} - (\overline{v'^2_o} - \overline{v'^2_{z_o}}) - \overline{v'^2_{Pe}} .$$

Now $\overline{v'^2} = \overline{v^2} - \bar{v}^2$, in general, and $\overline{v'^2_o} = \overline{v_o^2} = \bar{v}_o^2$, giving

$$\overline{v'^2_\theta} = (\overline{v^2} - \overline{v_o^2}) - (\bar{v}^2 - \bar{v}_o^2) - (\overline{v'^2_z} - \overline{v'^2_{z_o}}) - \overline{v'^2_{Pe}} .$$

Assume $\overline{v'^2_z} \approx \overline{v'^2_{z_o}}$, i.e., that the distributions of zero shift changes are the same whether there is flow or not (probably not a good assumption). This gives the final result

$$\overline{v'^2_\theta} = (\overline{v^2} - \overline{v_o^2}) - (\bar{v}^2 - \bar{v}_o^2) - \overline{v'^2_{Pe}} . \qquad (26)$$

The signals $\bar{v}^2$, $\overline{v^2}$, $\bar{v}_o^2$, and $\overline{v_o^2}$ are calculated from the digitized signals v and v_o, leaving only $\overline{v'^2_{Pe}}$ as an unknown. Equation (20)indicates that $\overline{v'^2_{Pe}}$ is independent of θ, so it is essentially a constant during the duration of a pulse. Thus the effect of $\overline{v'^2_{Pe}}$ is to shift the level of $\overline{v'^2_\theta}$. The correct magnitudes of $\overline{v'^2_\theta}$ can be obtained by measuring all voltages from this shifted level, which should be the signal level before the arrival of the heat pulse at the sensor. This process is illustrated in figure 9.

VI. THE PROBE CALIBRATION RESULTS

6.1 Velocity Measurements in Laminar Flow

Extensive calibration runs were made in both helium and air flows with one probe in order to determine that the probe did indeed operate as expected. In addition, the probe was recalibrated in air whenever a wire had been replaced.

The results were very poor when the half-amplitude point of the sensor output was used for the definition of the transit time t_o. The transit times in helium were always less than those in air; by a significant amount for some wires. By trial and error it was found that this peculiar behavior was not present when the point of maximum slope defined the transit time and the data scatter was reduced, even in those cases which had correlated well with the half-amplitude determined times.

The explanation for this became apparent later. In those cases where the calibrations for helium and air disagreed, the hot wire amplifiers apparently had been operated in an unbalanced state in an effort to minimize the wire current. The gain of the Miller M-5 hot wire amplifier is relatively low,as a result of which the current to a wire can be more than 1 mA even when the bridge resistances are set to operate the wire at its cold resistance. The current can be reduced by setting the bridge to operate the wire at a

resistance lower than its cold resistance. In such a condition the bridge is always unbalanced (greatly in some cases) which increases the response time of the circuitry. The resulting signals are something like those which would be obtained from an insufficiently compensated constant-current hot wire circuit and the effect is to change the measured delay by a function of the rise time of the signal. Interestingly, the time at which the point of maximum slope appears for an error-function-type signal processed by such a network is nearly independent of the response time of the electronics.

The rounding of the top of the pulse due to diffusion (molecular and turbulent) changes the apparent position of the half amplitude point, but the position of the point of maximum slope is practically unaffected. Since the use of the maximum slope point is valid also on theoretical grounds (cf. Sec. 2.2), it was used for all measurements.

Figure 10 plots the data for a typical probe calibration. Each data point is computed from a mean pulse shape, which is the average of about 100 pulses.* An even smaller number would be adequate for such laminar flows. A least squares fit of the data to a straight line of the form $t = t_d + \frac{t_o}{U}$ is made. The line does not pass through the origin because of a delay due to the finite response time

* The details of the computer calculations involved are given in Appendix B.

of the hot wire amplifiers, t_d. This delay, determined by the fitting process, is about 25 μs, but varies slightly depending on the amplifier and the bridge settings. Thus the correct transit time, t_o, is the measured time, t, less the response delay, t_d.

Figure 11 is a plot of the transit time t_o versus the velocity U for the data of figure 10. The scatter is on the order of 5%, which is a measure of the accuracy to be expected of the data in low-turbulence-level flows.

6.2 Velocity Measurements in Turbulent Flows

In order to determine the validity of equation (14), which gives the turbulence level in terms of the temperature fluctuations at t_m, several turbulent flows were measured with the probe. One of the probe sensing wires was operated in the usual way while an adjacent one was operated as a normal hot wire (i.e., at higher overheat) which was connected to a linearized hot wire anemometer. Turbulence levels were measured in the core of a jet, in the Kármán vortex street behind a circular cylinder, and in the turbulent region of a jet. The results are shown in figure 12.

The abscissa is the turbulence level determined by the single hot wire, without any correction for the effects of the v and w components. Without such corrections the reading is only an approximation of the true level. The ordinate is the turbulence level calculated from 200-400

pulses using equations (12) and (28). The calculations were performed on a digital computer according to the scheme described in appendix B. The figure shows that there is fair agreement between the hot wire and the heat pulse results for turbulence levels from 5% to 25%.

Low turbulence levels (< 3%) cannot be measured accurately because the voltage fluctuation levels $\sqrt{\overline{v'^2}}$, are on the order of one millivolt in such cases, which is the limit of resolution of the analog to digital conversion process. The presence of some noise which manages to elude all the corrections discussed in section 5.3 assures that the turbulence levels calculated from the probe data will have an error of about $\pm$ 0.03 for turbulence levels from 0 to 0.05.

The accuracy becomes poorer at turbulence levels above 30% also. As mentioned earlier, if the velocity component perpendicular to the mean flow direction is sufficiently large, the wake from the source wire can completely miss the sensing wire, which will result in an artificially high temperature fluctuation level. This will occur if this cross flow component is on the order of 0.5 U or greater, hence is to be expected if the turbulence intensities exceed, say, 0.3 for most types of flows. A mean flow which is highly inclined to the probe axis will also cause the reading of high turbulence levels.

Thus the turbulence levels calculated from the probe

data using equation (24) will be significantly higher than the true levels for, say, $\sqrt{\overline{u^2}}/\overline{U}$ greater than 0.4. The degree of error is unknown, however, because the single hot wire is a poor instrument for measuring such high turbulence levels. Because of this, the data in figure 12 can only be used to show that there is some merit to the analysis in the preceding sections.

Since the turbulence level also affects the measured value of the mean velocity through equation (10), the mean velocities determined in high turbulence levels, or in flows of large angularity with the probe axis, will be less than the true velocities. This means that data on the outer fringes of the jet will have poor accuracy.

The probe probably could be used in flows of higher turbulence levels if the source and sensing wires were both lengthened and if the series in u in section 2.4 retained the next higher order terms.

VII. THE RESULTS OF THE JET SURVEYS

The velocities and turbulence levels measured by the probe for the various combinations of gases discussed in section 4.3 enabled calculation of the width of the jet, the decay of velocity along the axis, and the turbulence level on the axis.

7.1 The Jet Width

The width of the jet, b, defined arbitrarily as the radial distance from the axis to the point at which the velocity is half of the velocity on the axis (Fig. 6) is a measure of the rate at which the jet flow entrains the external gas and spreads into it. Previous experimental data (Refs. 4 and 14) have shown that mean velocity profiles sufficiently far downstream from the nozzle have a shape like the normal probability curve, regardless of whether the flow is homogeneous or inhomogeneous. Consequently the experimental data, such as that shown in figure 13, were fitted to a profile shape of the form

$$\overline{U}(r) = \overline{U}_m \exp\left[-(\log 2)\left(\frac{r}{b}\right)^2\right] . \qquad (27)$$

The fitting was carried out by a computer program which minimized the mean square error from terms of the form $(\overline{U}(r) - \overline{U}_e(r))/\overline{U}(r)$ where $\overline{U}_e(r)$ is the experimentally determined value at r. The calculation gave b and $\overline{U}_m$ as output, as well as the root-mean-square scatter. If the

scatter was excessive, the "worst" point was discarded and the fitting was carried out again. If sensible results could not be obtained after a reasonable number of tries, the data were not used. (Spot checks usually showed an excessive number of "wild" data points in such profiles.)

Figure 13 displays the data obtained at x/d = 12 for the helium-air case. Most radial surveys do not contain data from all four nozzles, so the figure contains more data points than those used to define most profiles. With this exception, the data are representative of the profiles obtained in all flows. Listed on the figure are the values of b and $\overline{U}_m$ obtained by fitting the data for each nozzle to the profile shape of equation (27). These tabulated values of $\overline{U}_m$ were then used to obtain the values of $\overline{U}/\overline{U}_m$ plotted on the figure. A mean profile for all the nozzles is drawn through the data.

The scatter in the values of b for the various nozzles is representative of the usual data scatter. The value for d = 1/8", having been obtained from only six points, is the least reliable. The inability to reproduce exactly the same flow conditions from run to run is the main cause of the scatter in $\overline{U}/\overline{U}_m$. Another major cause of scatter, particularly toward the edges of the jet, is the coupling of the mean velocity to the velocity fluctuation level through equation (10). Measured fluctuation levels, such as those shown in the bottom portion of figure 13, show substantial

scatter at high levels. At these levels, $\overline{U}$ is a strong function of $\overline{u^2}/\overline{U}^2$, so this scatter also appears in the mean velocity. Although increasing the number of pulses sampled would decrease this scatter*, the values of $\overline{U}$ obtained for high fluctuation levels are not correct anyway because of the increasing significance of terms which were neglected in the expansions leading to equations (10) and (11).

Jet widths, obtained by fitting the experimental data to equation (27), are plotted in figure 14. (Near the nozzle, where the profiles have not yet reached the fully developed form, b was obtained visually from plots of $\overline{U}$.) Most of the points shown are averages of the widths obtained from flows from several nozzles of different diameters. For unknown reasons, the profiles for the 1/8" nozzle exhibited excessive scatter toward the fringes of the air-air jet in the far downstream region, so profile widths for this case could not be calculated for distances farther downstream than 24 diameters. The limited air-air data show reasonable agreement with results of previous research, the range of which is represented by the shaded region in the figure.

The qualitative observation from shadow photographs (Fig. 7) that a light jet should spread more rapidly initially than a heavy jet is confirmed by the data of figure

* Such an increase is not easily obtained, since the number of pulses during a run is constrained by the cooling rate of the wire between pulses and by the run duration limitation due to the recirculation of the jet gas.

14. Sufficiently far downstream, the jet should have entrained enough of the reservoir gas to make it behave essentially as a homogeneous jet. In this downstream region the growth rate of the jet should be that of a homogeneous jet with the same momentum flux, with the only effect of the density difference being a shift in the virtual origin of the flow. The He-SF_6 case shows this behavior for $x/d \gtrsim 10$. A similar result is probably true for He-air for $x/d \gtrsim 25$, but the absence of data points does not allow a definite conclusion to be made. The air-He case does not show a growth rate which is parallel to the homogeneous case by the farthest downstream point at $x/d = 48$, indicating that enough helium to achieve a nearly uniform density profile has not yet been entrained by this jet.

In the He-SF_6 case the jet has doubled in width by $x/d = 5$. Shadow photographs indicate that, in this case (Fig. 15), the jet spreads at very large angles to the axis for a short distance after breakdown of the initial shear layer. (A fraction of a nozzle diameter of the initial region is obscured in figure 15.)

Since the density differences between the jet gas and ambient gas are very large, the effect of buoyancy on the spreading rate and axial velocity decay should be considered. For the downward-flowing configuration of the present experiments, the effect of buoyancy would be to cause the light jet

to spread more rapidly and the heavy jet to spread less rapidly. For the velocities encountered in the present experiments, the effects of buoyancy can be shown to be sufficiently small so that it can be ignored. Appendix C discusses the buoyancy question in detail.

7.2 The Centerline Velocity Decay

The velocity along the centerline of a homogeneous jet decays as 1/x, as determined on theoretical grounds and verified by experiments. Figure 16 is a plot of the reciprocal of the centerline velocity, $\overline{U}_m$, normalized by the nozzle velocity, U_o. For the air-air case, this expression grows linearly with x/d after the initial region, as expected. The heavy (air-He) jet centerline velocity has barely decayed at all, being only half the nozzle value at x/d = 48, while the light jet velocities decay at a much faster rate, reaching 1/10 the nozzle value at x/d = 10 for the extreme case of helium flowing into sulfur hexafluoride. This again indicates a rapid rate of entrainment by the light jets. The dashed curve changes the scale by a factor of ten to allow the far downstream He-SF_6 points to be shown.

Two data points from the He-air experiments in reference 4 are also shown. They indicate a less rapid decay of velocity than does the present experiment. A line drawn through them is parallel to the present data, however. Since the experiment in reference 4 had a sharp-edged orifice, the

difference may be due to different virtual origins for the two experiments.

The velocity decay rate should reach that of a homogeneous jet sufficiently far downstream. As noted the velocity of a homogeneous jet decays as $1/x$, meaning $U_o/\bar{U}_m$ grows linearly with x. An inhomogeneous jet has reached the decay rate of the homogeneous jet when $U_o/\bar{U}_m$ for it grows linearly with x, also. The slope need not be the same, however. To see why this is true, consider the equation which equates the momentum at the nozzle with the momentum at some point, x, downstream:

$$\rho_o U_o^2 \pi r_o^2 = 2\pi \int_o^\infty \rho U^2 \, r \, dr \quad . \tag{28}$$

Far downstream, when $\rho \approx \rho_\infty$, the velocity profiles will have the same similarity form as the homogeneous jet:

$$\frac{\bar{U}}{\bar{U}_m} = f\left(\frac{r}{x - x_o}\right)$$

where x_o is the virtual origin for the flow. Averaging equation (28) for $\rho = \rho_\infty$, substituting the similarity profile, and non-dimensionalizing r with $x - x_o$ gives

$$\rho_o U_o^2 \left(\frac{r_o}{x - x_o}\right)^2 = 2\rho_\infty \bar{U}_m^2 \int_o^\infty f\left(\frac{r}{x - x_o}\right) \frac{r}{x - x_o} \, d\left(\frac{r}{x - x_o}\right) . \tag{29}$$

The integral has a constant value, say I, so equation (29) can be written in either of the two following forms:

$$\frac{\sqrt{\rho_o}U_o}{\sqrt{\rho_\infty}\bar{U}_m} = \sqrt{2I}\ \frac{x - x_o}{r_o} \tag{30}$$

or

$$\frac{U_o}{\bar{U}_m} = \sqrt{2I}\ \frac{x - x_o}{\sqrt{\frac{\rho_o}{\rho_\infty}}\, r_o} \tag{31}$$

The first form (Eq. (30)) says that, in the downstream region, the ratio $\frac{\sqrt{\rho_o}U_o}{\sqrt{\rho_\infty}\bar{U}_m}$ is described by the same function for all density ratios, except for an unknown coordinate origin, x_o. Since the momentum flux of the jet is proportional to $\rho_o \bar{U}_m^{\,2}$ in this region, the ratio under discussion is proportional to the reciprocal of the jet momentum flux.

The second expression (Eq. (31)) says that, if $\frac{U_o}{\bar{U}_m}$ were plotted against a scaled coordinate x/r_e, where $r_e = \frac{\sqrt{\rho_o}}{\sqrt{\rho_\infty}}\, r_o$, the data for all density ratios would coincide on one straight line for sufficiently large x/r_e, if x_o was the same for all cases. Since x_o varies, a set of parallel lines should result.

Differentiation of either equation (30) or (31) gives

$$\frac{d}{dx}\frac{U_o}{\bar{U}_m} = \frac{\sqrt{2I}}{r_o}\sqrt{\frac{\rho_\infty}{\rho_o}}\ ,$$

confirming the earlier statement that the slopes of U_o/U_m for the various gas combinations would not approach the same value. This equation shows that the slope is least for the heavy jet and greatest for the light jet, as figure

16 indicates.

Equations (30) and (31) both indicate that the final state of the jet depends only on the initial momentum flux, but they indicate different ways in which this momentum flux could be obtained. In particular, the scaling of the lengths with the ratio $\sqrt{\rho_o/\rho_\infty}$ simply says that a jet of density ρ_o flowing at velocity U_o through a nozzle of radius r_o can be replaced, as far as the downstream flow is concerned, by a homogeneous jet flowing at the same velocity through a nozzle of radius r_e. That this should be so is clear, since the momenta of both jets are the same:

$$\rho_o U_o^2 \pi r_o^2 \equiv \rho_\infty U_o^2 \pi r_e^2 \quad .$$

In figure 17 the data of figure 16 have been replotted on a graph in which the abscissa has been scaled in the way suggested by equation (31). (To avoid crowding most of the data, three of the He-SF_6 points at $x/d > 100$ are not shown. Still, all of the air-He data are compressed into the lower left corner of the graph. The dashed line is an extension of a straight line passing through the three deleted points.) The slopes are nearly the same, so the curves would coincide, except for a shift in virtual origin. The location of the virtual origin shows no obvious correlation with ρ_o/ρ_∞, which may be because the different gases were run at different nozzle Reynolds numbers.

7.3 The Velocity Fluctuation Level

Values of $\sqrt{u^2}/\bar{U}$ at x/d = 12 for the He-air jet are shown in figure 13, and fluctuation level values along the axis of the homogeneous jet are plotted in figure 18. The data from the various nozzles are shown to indicate the relatively good agreement between readings over most of the jet, the scatter being the greatest in the initial region and at the edge of the jet. The dashed curve in figure 18 was obtained by Corrsin (Ref. 1). Three points from the recent, very thorough study of Wygnanski and Fiedler (Ref. 15) are also shown. The data from the probe are higher everywhere than the data of Corrsin or of Wygnanski and Fiedler, but the general trend is similar enough that comparisons between fluctuation levels in different flows would be meaningful.

A comparison of the same quantity for the various gas combinations is shown in figure 19. The air-air curve is that of figure 18, and the data points for the other cases are again averages for the several nozzle diameters.

The same type of behavior appears here as in the velocity and width comparisons. The lowest fluctuation levels, indicating the smallest rate of entrainment of the reservoir gas by the jet, are shown by the air-helium case. The fluctuation level of the He-SF_6 jet rises most rapidly, indicating a rapid entrainment rate at very short distances

downstream of the nozzle. For both light jets the fluctuation level overshoots and then drops toward a lower level as the distance downstream increases.

All turbulence levels should eventually reach the same value sufficiently far downstream. The curves drawn through the points indicate how this might occur. The distance in which the turbulence level reaches that of the homogeneous jet is a measure of the distance required to reach the homogeneous state, in which the nozzle gas composition no longer matters. The data plotted in figure 17 show this distance to be about $x/d \approx 25$ for He-SF_6 and, $x/d > 40$ for He-air and $x/d > 60$ for air-He. These distances are greater than those obtained from the growth rate of the jet (Sec. 7.2 and Fig. 14) or those that would be deduced from the axial velocity decay (Fig. 16). This is consistent with the observations of Wygnanski and Fiedler (Ref. 15) that the turbulence level is the most sensitive measure of the approach to self-preservation.

The general observation can thus be made that the light jet reaches the homogeneous state first, but enough data does not exist to arrive at any quantitative relation for the distance in which this will occur for any given density ratio.

The variation of the centerline fluctuation level distribution over such a wide range of density ratios is

quite small. Because of this it is not at all surprising that Corrsin (Ref. 1) could find no difference in the turbulent fields of the homogeneous and heated jets. His greatest density ratio (0.61) was too small to show any effect.

VIII. CONCLUSIONS

8.1 The Velocity Measurement Technique

The experiments indicate that the heat-pulse velocity measuring probe is capable of measuring the mean velocity in a moderately turbulent stream of unknown composition with reasonable accuracy. The accuracy of fluctuation level measurements made by the probe seem to be fair, but more careful testing is required to determine the reliability of such measurements.

The accuracy would certainly be helped by some modifications of the probe and associated equipment. The large voltage excursion causing the ringing of the tape recorder amplifiers should be eliminated before it reaches the tape recorder. This would significantly improve the accuracy of measurements at the higher speeds. Particular care needs to be taken to minimize all electrical noise, so that the signal-to-noise ratio of the differentiated signal is as large as possible, and so that the measured voltage fluctuation levels are as accurate as possible.

There are two conflicting requirements for the spacing between the source wire and the sensing wires on the probe. The transit times are most easily and accurately measured if the wire spacing is such that t_m is in the range 100 to 500 μs, so that a probe with larger wire spacing would be desirable for measurement of high velocities. On the other hand,

it would be desirable to have the source and sensing wires as close together as possible, in order to facilitate measurements of as small scale fluctuations as possible. The optimum solution is a large scale experiment, so that the turbulence scale is large and so that reasonable Reynolds numbers can be achieved without requiring such large velocities that the heat pulse transit times become very short.

An inspection of the equations shows that t_o and t_m are negligibly different if the turbulence level is below 10%, so one of the easier applications for the probe appears in low turbulence flows of unknown composition, such as boundary layers with gas injection at the wall. For such conditions a photograph of several superimposed oscilloscope traces of the differentiated sensing wire signal is sufficient to enable measurement of the transit time, and computer processing is completely unnecessary for mean velocity determination.

The field of digital data acquisition and data handling is rapidly becoming an important research technique. Since it is not a very familiar field to many researchers, some comments about it may be in order. The main advantage of digital techniques is the ability to handle enormous volumes of data and to acquire and process this data much more rapidly than by any other method. For example, the effective data acquisition rate for the present experiment was 800,000 numbers per second and the total amount of data processed

amounted to more than 90 x 10^6 numbers. The major disadvantage of digital techniques is the high cost of the electronic equipment involved. Another disadvantage of the scheme used in this experiment (viz., analog data recording, analog-to-digital conversion, and digital data processing) was the uncomfortably long time between the experimental runs and the appearance of the final data. Most of this long time was occupied by several weeks of analog-to-digital conversion and several months of program "debugging". If an analog-to-digital converter is readily available and the programs required are already working properly, it should be possible to obtain data within a few days of the experiment.

It is possible to dispense with the analog tape recording and to calculate the required temperature profile shapes concurrently with the running of the experiment by using a small instrumentation computer. Such a computer, which costs about the same as a good tape recorder, can digitize the signals from the sensing wire, calculate the required products and averages, and then store the resulting arrays of numbers for display on a digital display oscilloscope or for recording on digital tape for further processing with a general purpose computer. At the time this is being written, an "off-the-shelf" computer which could perform the data acquisition and calculation required for the present experiment does not appear to be available. None of the computers known to the writer is capable of performing the

digitization and calculations at a sufficiently rapid rate and with sufficient accuracy to match the 10 bit resolution (1 part in 1024) and 200 kHz data rate obtained in the present experiment by using the tape recorder as a time-scaling device. However, the specifications of present instrument computers are quite adequate for the same type of calculations in slower flow (allowing a lower sampling frequency and calculation rate) with longer running times (so that averaging of a greater number of signals will increase the accuracy to compensate for poorer resolution). The state-of-the-art for small computers is changing so rapidly that significantly higher sampling rates and greater resolution will certainly be possible within a few years.

8.2 The Velocity Measurements

The surveys of the flows for various jet and ambient density combinations allowed calculation of several complementary and self-consistent sets of information about the velocity field of the inhomogeneous turbulent jet. In summary, compared to the inhomogeneous jet, a light jet has a shorter initial region of flow development, which is followed by a more rapid spreading and velocity decay. The axial velocity fluctuation level rises more rapidly than that of the inhomogeneous jet, overshoots the final level slightly and then slowly approaches the final, self-preserving, fluctuation level. All of this indicates a region of

high entrainment following the initial portion of a light jet, which, in turn, leads to a rapid approach to the near-homogeneous jet. In contrast, the heavy jet remains in an inhomogeneous state for a much longer distance, as indicated by the low axial turbulence levels, the slow spreading rate, and the slow decrease in axial velocity.

For completeness, these experimental measurements should be extended farther downstream for the heavy jet, and more measurements should be made near the nozzle for all cases at various Reynolds numbers. This should enable a more quantitative prediction of the length of the initial portion of the flow as a function of the density ratio than was possible from the present data,which would be useful for many engineering applications.

APPENDIX A

CALCULATION OF TRANSIT TIME AND FLUCTUATION LEVEL IN TURBULENT FLOW

The mean heat pulse temperature profile in turbulent flow, $\overline{\theta}(t, U)$, can be expressed in terms of the single profile, $\theta(t, \overline{U})$, which would be obtained in laminar flow at the mean velocity $\overline{U}$. Let $U = \overline{U} + u$, where $\overline{U}$ is the mean velocity and u is a fluctuation due to a large eddy, and write $\theta(t, U)$ in a Taylor series in u:

$$\theta(t, U) = \theta(t, \overline{U}) + \frac{\partial\theta}{\partial U}(t, \overline{U})\, u + \frac{1}{2}\frac{\partial^2\theta}{\partial U^2}(t, \overline{U})\, u^2 + \frac{1}{6}\frac{\partial^3\theta}{\partial U^3}(t, \overline{U})\, u^3 + \frac{1}{24}\frac{\partial^4\theta}{\partial U^4}(t, \overline{U})\, u^4 + O(u^5).$$

Averaging over all U, letting $\theta = \overline{\theta} + \theta'$, gives

$$\overline{\theta(t, U)} = \theta(t, \overline{U}) + \frac{1}{2}\frac{\partial^2\theta}{\partial U^2}(t, \overline{U})\, \overline{u^2} + \frac{1}{24}\frac{\partial^4\theta}{\partial U^4}(t, \overline{U})\, u^4 + O(\overline{u^6}) \qquad \text{(A-1)}$$

and

$$\theta'(t, U) = \frac{\partial\theta}{\partial U}(t, \overline{U})\, u + \frac{1}{6}\frac{\partial^3\theta}{\partial U^3}(t, \overline{U})\, u^3 + O(u^5) \quad ,$$

hence

$$\overline{[\theta'(t,U)]^2} = \left[\frac{\partial\theta}{\partial U}(t, \bar{U})\right]^2 \overline{u^2}$$

$$+ \frac{1}{6}\frac{\partial\theta}{\partial U}(t, \bar{U})\ \frac{\partial^3\theta}{\partial U^3}(t, \bar{U})\ \overline{u^4} + O(\overline{u^6}). \qquad \text{(A-2)}$$

In the vicinity of the half amplitude point in the θ-profiles of section 2.1 and 2.3, it can be shown that $\frac{\partial\theta}{\partial U} = \frac{t}{U}\frac{\partial\theta}{\partial t}$. Assume a normal distribution for u, so $\overline{u^4} = 3(\overline{u^2})^2$. Using these relations, equations (A-1) and (A-2) become

$$\overline{\theta(t, U)} = \theta(t, \bar{U}) + \frac{1}{2}t^2\frac{\partial^2\theta}{\partial t^2}(t, \bar{U})\ \frac{\overline{u^2}}{\bar{U}^2}$$

and
$$+ \frac{1}{8}t^4\frac{\partial^4\theta}{\partial t^4}(t, \bar{U})\left(\frac{\overline{u^2}}{\bar{U}^2}\right)^2 + O\left(\frac{\overline{u^2}}{\bar{U}^2}\right)^3 \qquad \text{(A-3)}$$

$$\overline{[\theta'(t, U)]^2} = \left[t\frac{\partial\theta}{\partial t}(t, \bar{U})\right]^2 \frac{\overline{u^2}}{\bar{U}^2}$$

$$+ \frac{1}{2}t^4\frac{\partial\theta}{\partial t}(t,\bar{U})\ \frac{\partial^3\theta}{\partial t^3}(t,\bar{U})\left(\frac{\overline{u^2}}{\bar{U}^2}\right)^2 + O\left(\frac{\overline{u^2}}{\bar{U}^2}\right)^3. \qquad \text{(A-4)}$$

Differentiation of equation (A-3) at t_o gives

$$\frac{\partial^2\theta}{\partial t^2}(t_o, U) = 2\,t_o\frac{\partial^3\theta}{\partial t^2}(t_o, \bar{U})\ \frac{\overline{u^2}}{\bar{U}^2} + O\left(\frac{\overline{u^2}}{\bar{U}^2}\right)^2,$$

which is a negative number. So the peak slope of $\bar{\theta}$ is not at t_o. Define t_m as the time at which the peak slope of $\bar{\theta}$ does occur, i.e.,

$$\frac{\partial^2\bar{\theta}}{\partial t^2}(t_m, U) = 0$$

To determine the mean velocity $\bar{U} = \ell/t_o$ it is necessary to calculate the relationship between t_m and t_o. A double Taylor series expansion of θ about $\bar{U} = U - u$ and $t_m = t_o + t'$ gives

$$\overline{\theta(t_o, U)} = \theta(t_m, \bar{U}) + \frac{\partial\theta}{\partial t}(t_m, \bar{U})\, t' + \frac{1}{2}\frac{\partial^2\theta}{\partial t^2}(t_m, \bar{U})\, t'^2$$
$$+ \frac{1}{2} t_m^2 \frac{\partial^2\theta}{\partial t^2}(t_m, \bar{U})\, t' + \frac{1}{2}\frac{\partial^2\theta}{\partial t^2}(t_m, \bar{U})\, t'^2$$
$$+ \frac{1}{2} t_m^2 \frac{\partial^2\theta}{\partial t^2}(t_m, \bar{U})\frac{\overline{u^2}}{\bar{U}^2} + \frac{1}{2} t_m^2 \frac{\partial^3\theta}{\partial t^3}(t_m, \bar{U})\frac{\overline{u^2}}{\bar{U}^2}\, t'$$
$$+ \frac{1}{8} t_m^4 \frac{\partial^4\theta}{\partial t^4}(t_m, \bar{U})\left(\frac{\overline{u^2}}{\bar{U}^2}\right)^2 + \ldots \quad ,$$

where the relations $\frac{\partial\theta}{\partial U}(t_m, \bar{U}) = \frac{t_m}{\bar{U}}\frac{\partial\theta}{\partial t}(t_m, \bar{U})$ and the assumption of a normal distribution in u (implying $\overline{u^4} = 3\left[\overline{u^2}\right]^2$) have been used. A Taylor series for θ about t_m is

$$\theta(t_o, \bar{U}) = \theta(t_m, \bar{U}) + \frac{\partial\theta}{\partial t}(t_m, \bar{U})\, t' + \frac{1}{2}\frac{\partial^2\theta}{\partial t^2}(t_m, \bar{U})\, t'^2 + \ldots$$

Combining the above equations, since $\theta(t_o, \bar{U}) = \overline{\theta(t_o, U)}$, gives

$$\frac{\partial^2\theta}{\partial t^2}(t_m, \bar{U}) + \frac{\partial^3\theta}{\partial t^3}(t_m, \bar{U})\, t' + \frac{1}{4} t_m^2 \frac{\partial^4\theta}{\partial t^4}(t_m, \bar{U})\frac{\overline{u^2}}{\bar{U}^2} + \ldots = 0. \qquad \text{(A-5)}$$

Differentiating equation (A-3) twice gives

$$\frac{\partial^2\overline{\theta}}{\partial t^2}\,(t_m,\ U) = 0 = \frac{\partial^2\theta}{\partial t^2}\,(t_m,\ \overline{U})$$

$$+\left\{\frac{\partial^2\theta}{\partial t^2}\,(t_m,\ U) + 2t_m\,\frac{\partial^3\theta}{\partial t^3}\,(t_m,\ U)\right.$$

$$\left. + \frac{1}{2}\,t_m{}^2\,\frac{\partial^4\theta}{\partial t^4}\,(t_m)\right\}\,\frac{\overline{u^2}}{\overline{U}^2} + \ldots$$

enabling $\frac{\partial^4\theta}{\partial t^4}\,(t_m,\ \overline{U})$ to be eliminated from equation (A-5). Also

$$\frac{\partial^2\theta}{\partial t^2}\,(t_o,\ \overline{U}) = 0 = \frac{\partial^2\theta}{\partial t^2}\,(t_m,\ \overline{U}) + \frac{\partial^3\theta}{\partial t^3}\,(t_m,\ \overline{U})\ t' + \ldots\ ,$$

enabling elimination of $\frac{\partial^3\theta}{\partial t^3}\,(t_m,\ \overline{U})$ from the resulting equation. The equation that remains has $\frac{\partial^2\theta}{\partial t^2}\,(t_m,\ \overline{U})$ as a common factor. Since $\frac{\partial^2\theta}{\partial t^2}\,(t_m,\ \overline{U})$ is non-zero, the entire equation can be divided by it, leaving

$$t' + (t' - 2\ t_m)\ \frac{\overline{u^2}}{\overline{U}^2} = 0 + \ldots\ ,$$

which solves for t' as

$$t' + \frac{2t_m}{1 + \frac{\overline{u^2}}{\overline{U}^2}}\,\frac{\overline{u^2}}{\overline{U}^2} + O\left(\frac{\overline{u^2}}{\overline{U}^2}\right)^3 \quad .$$

So

$$t_o = t_m\left(1 + \frac{2\,\frac{\overline{u^2}}{\overline{U}^2}}{1+\frac{\overline{u^2}}{\overline{U}^2}}\right) + O\left(\frac{\overline{u^2}}{\overline{U}^2}\right)^3 \quad . \qquad \text{(A-6)}$$

The fluctuation level $\frac{\overline{u^2}}{\bar{U}^2}$ can be calculated from equation (A-4), evaluated at t_m, by assuming $\overline{u^4} = 3(\overline{u^2})^2$, and using the first derivative of equation (A-3) at t_m to replace $\frac{\partial\theta}{\partial t}$ by $\frac{\partial\bar{\theta}}{\partial t}$. The equation which is obtained is

$$\overline{\theta'^2(t_m,U)} = t_m^2\left[\frac{\partial\bar{\theta}}{\partial t}(t_m,U)\right]^2\frac{\overline{u^2}}{\bar{U}^2} - 2\frac{\partial\bar{\theta}}{\partial t}(t_m,U)\frac{\partial^2\theta}{\partial t^2}(t_m,\bar{U})t_m^3\left(\frac{\overline{u^2}}{\bar{U}^2}\right)^2$$

$$+ t_m^4\frac{\partial^3\theta}{\partial t^3}(t_m,\bar{U})\left[\frac{\partial\theta}{\partial t}(t_m,\bar{U}) - \frac{\partial\bar{\theta}}{\partial t}(t_m,U)\right]\left(\frac{\overline{u^2}}{\bar{U}^2}\right)^2$$

$$+ O\left(\frac{\overline{u^2}}{\bar{U}^2}\right)^3 .$$

The difference term in square brackets is of order $\overline{u^2}/\bar{U}^2$ and $\frac{\partial^2\bar{\theta}}{\partial t^2}(t_m,U) = 0 = \frac{\partial^2\theta}{\partial t^2}(t_m,\bar{U}) + O\left(\frac{\overline{u^2}}{\bar{U}^2}\right)$

so

$$\overline{\theta'^2(t_m,U)} = t_m^2\frac{\partial\bar{\theta}}{\partial t}(t_m,U)\frac{\overline{u^2}}{\bar{U}^2} + O\left(\frac{\overline{u^2}}{\bar{U}^2}\right)^3 .$$

Solving for the fluctuation level, this gives

$$\frac{\overline{u^2}}{\bar{U}^2} = \frac{\theta'^2(t_m,U)}{t_m^2\left[\frac{\partial\bar{\theta}}{\partial t}(t_m,U)\right]^2} + O\left(\frac{\overline{u^2}}{\bar{U}^2}\right)^3 . \qquad \text{(A-7)}$$

After obtaining the fluctuation level from equation (A-7), the transit time, t_o, can be calculated by using equation (A-6) and the mean velocity then follows from $\bar{U} = \ell/t_o$.

APPENDIX B

DETAILS OF THE COMPUTER DATA REDUCTION PROCEDURES

The analog data from the experimental runs was digitized as discussed in section 5.1. The digitized data were written on to digital tape by an IBM 7040 computer, where they were stored for later data reduction. The actual data reduction was carried out by an IBM 7040-7094 computer pair. Two passes were made over all sets of the data. The first run calculated the appropriate averages of the voltages and stored them, along with identifying labels and various numbers denoting the amount of data, the sampling rate, etc., on a second reel of computer tape. The data on the second reel were then used for calculating the time delays and velocities. Some details of the various computing processes are described below.

B.1 The Averaging Run

The raw digitized data were read into the core of the computer, one pulse at a time. In addition to the voltages of all the samples during one pulse, the squares of all the voltages were also stored. Each succeeding pulse was then treated the same way, and the results were added to those for the corresponding points of the preceding pulses. The resulting stored arrays of sums of voltages and sums of squares of voltages were then divided by the number of pulses to obtain the $\bar{v}$ and $\overline{v^2}$ discussed in section 5.3.

The signals recorded in the absence of any flow, containing the ringing, were processed identically.

The values of $\bar{v}$ and $\overline{v^2}$ thus obtained were stored on a second digital tape. The rate at which data could be averaged was determined by the tape reading rate, averaging about one second per run.

B.2 The Calibration Calculation

For the data from the laminar calibration flows the first operation performed was the reading of the mean no-flow voltages, $\bar{v}_o$, from the second digital tape. The values of $\bar{v}_o$ for all four wires were stored in the computer core for further use.

The values of $\bar{v}$ for a particular calibration run were then read from the tape into the computer core. The values of $\bar{v}_o$ were subtracted for corresponding points, and the resulting set of values for $\bar{v} - \bar{v}_o$ was smoothed by evaluating at each point the least-squares polynomial of degree 3 relevant to the five successive points centered on the point being smoothed. The purpose of the smoothing was to further eliminate any residual effects of the ringing and to sufficiently smooth the pulse shape to enable calculation of a meaningful derivative.

The smoothed set of values for $\bar{v} - \bar{v}_o$ was differentiated by calculating at each point the derivative of the Lagrangian interpolation polynomial of degree two relevant

to the three successive points centered on the point for which the derivative was being calculated. The data for $\frac{d}{dt}(\bar{v} - \bar{v}_o)$ is also smoothed by the same process as used for the profile data.

The computer then scanned the set of values for $\frac{d}{dt}(\bar{v} - \bar{v}_o)$, starting from the last point and working forward, searching for the maximum value. Maxima which were less than six points from the front data point, as well as those which had a point with a value less than or equal to zero (corresponding to negative or zero slope in the voltage data) within two points to either side were rejected. In the event that there existed two separated points with values within 1% of each other, the point corresponding to a shorter delay was used, and an "error index" was set to a non-zero value.

In order to check the validity of the point at which the computer had determined the maximum slope to be, the time at which the amplitude of the pulse profile was half its peak value was obtained by a similar scanning process. If the half amplitude point was ahead of the peak slope point, another error index was set to a non-zero value. (Experience has shown that such a condition nearly always meant an error in the calculation.)

The computer then calculated the time delay, $t_m = t_o + t_d$, corresponding to the point at which it had

determined the maximum slope occurred. If an error index had been set to a non-zero value, plots of smoothed values of $\overline{v} - \overline{v}_o$ and $\frac{d}{dt}(\overline{v} - \overline{v}_o)$ were produced on the printer for visual verification of the correctness of the calculation.

In the absence of the necessity to do the plotting, a typical delay calculation required about 0.2 seconds. Plotting added an additional 2 to 5 seconds to the computation time.

The times thus calculated, as well as the corresponding velocities obtained from a pitot tube, were used for calculation of the wire spacing ℓ and the amplifier delay time t_d. The least-square fit of a line of the form $1/U = t_d + \ell t_o$ to the data was performed later on another computer, the Caltech developed CITRAN system (an on-line time-sharing system using the IBM 360-50 computer). CITRAN was also used for the profile curve fits discussed in section 7.1.

B.3 The Turbulent Flow Velocity Calculations

For the velocity measurement data obtained for the turbulent inhomogeneous flows the data processing scheme followed the pattern used for the calibrations, except that there was more calculation involved.

The no-flow signal calculation was carried out exactly as for the calibrations. In addition the values of $\overline{v_o^2}$ were read from the tape, and the quantity $\overline{v_o^2} - \overline{v}_o^2$ was calculated

and stored for each point. At this time, too, the amplifier delay, t_d, and the wire spacing, ℓ, were read in from punched cards.

The pulse profile voltages were then read and a transit time, t_m, was calculated as for the calibrations. In addition the maximum value of $\frac{d}{dt}(\bar{v} - \bar{v}_o)$ was noted and stored. Then $\overline{v^2}$ was read from the tape and the mean square fluctuation level $\overline{v^2} - \bar{v}^2$ was calculated at each point. The corresponding expression for the no-flow signal was subtracted from this, giving $(\overline{v^2} - \overline{v_o^2}) - (\bar{v}^2 - \bar{v}_o^2)$ (cf. equation (26)). This set of squared fluctuation level data was then smoothed in the usual way.

The "hot wire effect" term $\overline{v'^2_{Pe}}$ (Eq. (26)) was set at the value of the smoothed data around the point where the slope $\frac{d}{dt}(\bar{v} - \bar{v}_o)$ was zero or negative closest to the front of the peak slope point. This corresponded to the value of $(\overline{v^2} - \overline{v_o^2}) - (\bar{v}^2 - \bar{v}_o^2)$ before the arrival of the temperature pulse. This value was then subtracted from the squared fluctuation level value at the point corresponding to the point of maximum slope, giving $\overline{v'^2_\theta}$ (Fig. 10). Division by the squares of $t_m = t_M - t_d$ and the maximum slope gives the velocity fluctuation level $\frac{\overline{u^2}}{\bar{U}^2}$ (Eq. (24)). The calculation of t_o and $\bar{U}$ is then straightforward, using equations (10) and (23).

A typical computation of this type requires 0.3 seconds, unless plotting is required. Plotting adds 3-6 seconds.

APPENDIX C

THE EFFECT OF BUOYANCY

Since the jet density in this experiment often differs greatly from the ambient density, the buoyancy of the light gas relative to the heavier one could have a significant effect on the jet spreading and velocity decay. An estimate of the effect of the buoyancy can be made by equating the axial rate of change of the jet momentum to the mean buoyant force on the jet:

$$\frac{dM}{dx} = 2\pi g \int (\bar{\rho} - \rho_\infty)\, r\, dr \quad .$$

Non-dimensionalizing this equation with the original jet momentum, $M_o = \frac{1}{4}\pi \rho_o u_o^2 d^2$, and the jet width, gives

$$\frac{1}{M_o}\frac{dM}{d(x/d)} = 8\,\frac{gd}{u_o^2}\left(\frac{b}{d}\right)^2 \left(1 - \frac{\rho_\infty}{\rho_o}\right)\int \bar{c}\,\frac{r}{b}\,d\left(\frac{r}{b}\right) \qquad \text{(C-1)}$$

where $\bar{c} = \dfrac{\bar{\rho} - \rho_\infty}{\rho_o - \rho_\infty}$ is the jet fluid concentration $(0 \leq c \leq 1)$.

To evaluate the right side of equation (C-1) it is necessary to estimate the value of the integral. The experiments in reference 4 show that $\bar{c}$ can be represented by a normal probability curve whose width is of the same order (i.e., within a factor of 2) as b, and whose peak value, $\bar{c}_m(x)$, varies as 1/x. In that case

$$\int \bar{c}\,\frac{r}{b}\,d\left(\frac{r}{b}\right) \propto \bar{c}_m(x)$$

when the constant of proportionality is approximately equal to unity. Then

$$\frac{1}{M_o}\frac{dM}{d(x/d)} \approx 8\,\frac{gd}{u_o^2}\left(\frac{b}{d}\right)^2\left(1-\frac{\rho_\infty}{\rho_o}\right)\bar{c}_m \quad .$$

Now, from reference 4, $\bar{c}_m \sim 10(x/d)$ for $x/d \gtrsim 10$, over a wide range of density ratios. From figure 14 it can be seen that $\frac{b}{d} \sim 0.1\,\frac{x}{d}$, so

$$\frac{1}{M_o}\frac{dM}{d(x/d)} \approx 0.8\,\frac{gd}{u_o^2}\left(1-\frac{\rho_\infty}{\rho_o}\right)\frac{x}{d} \quad .$$

Thus, the effect of buoyancy is greatest for large x/d, where the velocities are the smallest. The strongest effect occurs for $\rho_\infty >> \rho_o$, viz., for He-SF_6 where $\frac{\rho_\infty}{\rho_o} = 36.5$. For this case, u_o was 8400 cm/s for d = 1/8", so

$$\frac{1}{M_o}\frac{dM}{d(x/d)} \approx -10^{-4}\,\frac{x}{d} \quad . \qquad \text{(C-2)}$$

An integration of equation (C-2) along the length of the jet gives an approximation to the total change in jet momentum due to buoyancy:

$$\frac{M - M_o}{M_o} = \frac{1}{M_o} \int_o^{x/d} \frac{dM}{d(x/d)} \, d\left(\frac{x}{d}\right)$$

$$\approx -\frac{1}{2} \times 10^{-4} \left(\frac{x}{d}\right)^2 .$$

At $x/d = 48$ this is $\frac{M - M_o}{M_o} \approx -.1$. So, the momentum of the $He\text{-}SF_6$ jet has decreased by about 10% in 48 diameters. This corresponds to a 5% change in the jet velocity, which, although not negligible, is small enough not to alter the data noticeably. For smaller x/d the buoyancy effect is, of course, much less. A similar calculation for the He-air case gives $\frac{M - M_o}{M_o} \approx -.01$, which is smaller than the accuracy of the measurements.

REFERENCES

1. Corrsin, S., "I. Extended Applications of the Hot Wire Anemometer. II. Investigations of the Flow in Round, Turbulent Jets", Ph.D. Thesis, California Institute of Technology (1947).

2. Corrsin, S., "Investigation of the Flow in an Axially Symmetric Heated Jet of Air", NACA Wartime Report W-94 (1943).

3. Corrsin, S., and Uberoi, M. S., "Further Experiments on the Flow and Heat Transfer in a Heated Turbulent Air Jet", NACA Technical Report 998 (1949).

4. Keagy, W. R., and Weller, A. E., "A Study of Freely Expanding Inhomogeneous Jets", Proceedings of the Heat Transfer and Fluid Mechanics Institute, Berkeley, California, 89 (1949).

5. Eggers, J., "Velocity Profiles and Eddy Viscosity Distribution Downstream of a Mach 2.22 Nozzle Exhausting to Quiscent Air", NASA Technical Note D-3601 (1966).

6. Conger, W. L., "The Measurement of Concentration Fluctuations in the Mixing of Two Gases by Hot-Wire Anemometer Techniques", Ph.D. Thesis, University of Pennsylvania (1965).

7. Aihara, Y., Kassoy, D.R., and Libby, P.A., "Heat Transfer from Circular Cylinders at Low Reynolds Numbers. II. Experimental Results and Comparison with Theory", Phys. Fluids 10, 947 (1967).

8. Kassoy, D. R., "Heat Transfer from Circular Cylinders at Low Reynolds Numbers. I. Theory for Variable Property Flow", Phys. Fluids 10, 938 (1967).

9. Kovasznay, L. S. G., "Hot-Wire Investigation of the Wake behind Cylinders at Low Reynolds Numbers", Proc. Roy. Soc. of London, A, 198, 174 (1949).

10. Bauer, A. B., "Direct Measurement of Velocity by Hot-Wire Anemometry", AIAA J., 3, 1189 (1965).

11. Bauer, A. B., "Final Report--Instrumentation Development for the Base Flow Region of a Multinozzle Booster Vehicle", Aeronutronic Division, Philco Corp., Publication No. U-3363 (1966).

REFERENCES (cont'd.)

12. Morse, P. M., and Feshbach, H., Methods of Theoretical Physics, McGraw Hill Book Co., New York, 859 (1953).

13. Carslaw, H. S., and Jaeger, J. C., Conduction of Heat in Solids, Oxford University Press, London, 218 (1947).

14. Albertson, M. L., et al., "Diffusion of Submerged Jets", Trans. ASCE, 115, 639 (1950).

15. Wygnanski, I., and Fiedler, H. E., "Some Measurements in the Self Preserving Jet", Boeing Scientific Research Laboratories Document D1-82-0712, (1968).

16. Schlichting, H., Boundary Layer Theory, 4th ed., McGraw Hill Book Co., New York, 607 (1960).

Track	Mode	Signal
1-4	FM	Sensor output (amplified x 600 and AC-coupled)
5	FM	Flow monitor
6	FM	Gas-composition monitor
7	FM	Control oscilloscope gate signal (x 0.1)
8	Direct	Recorder servo signal
9	Direct	Pulser Signal
Edge	Direct	Voice identification

Table 1. Summary of Recorded Data

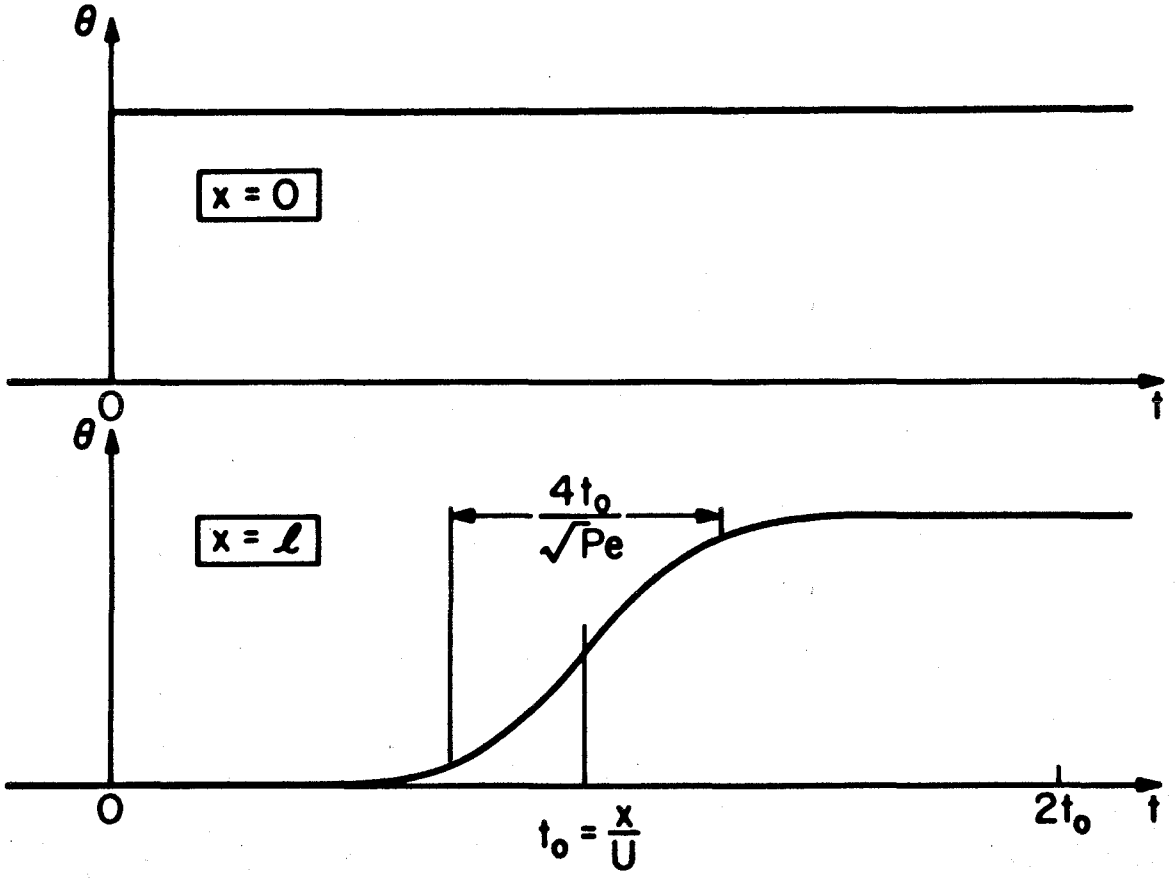

Figure 1. Ideal behavior of a temperature jump in a uniform stream.

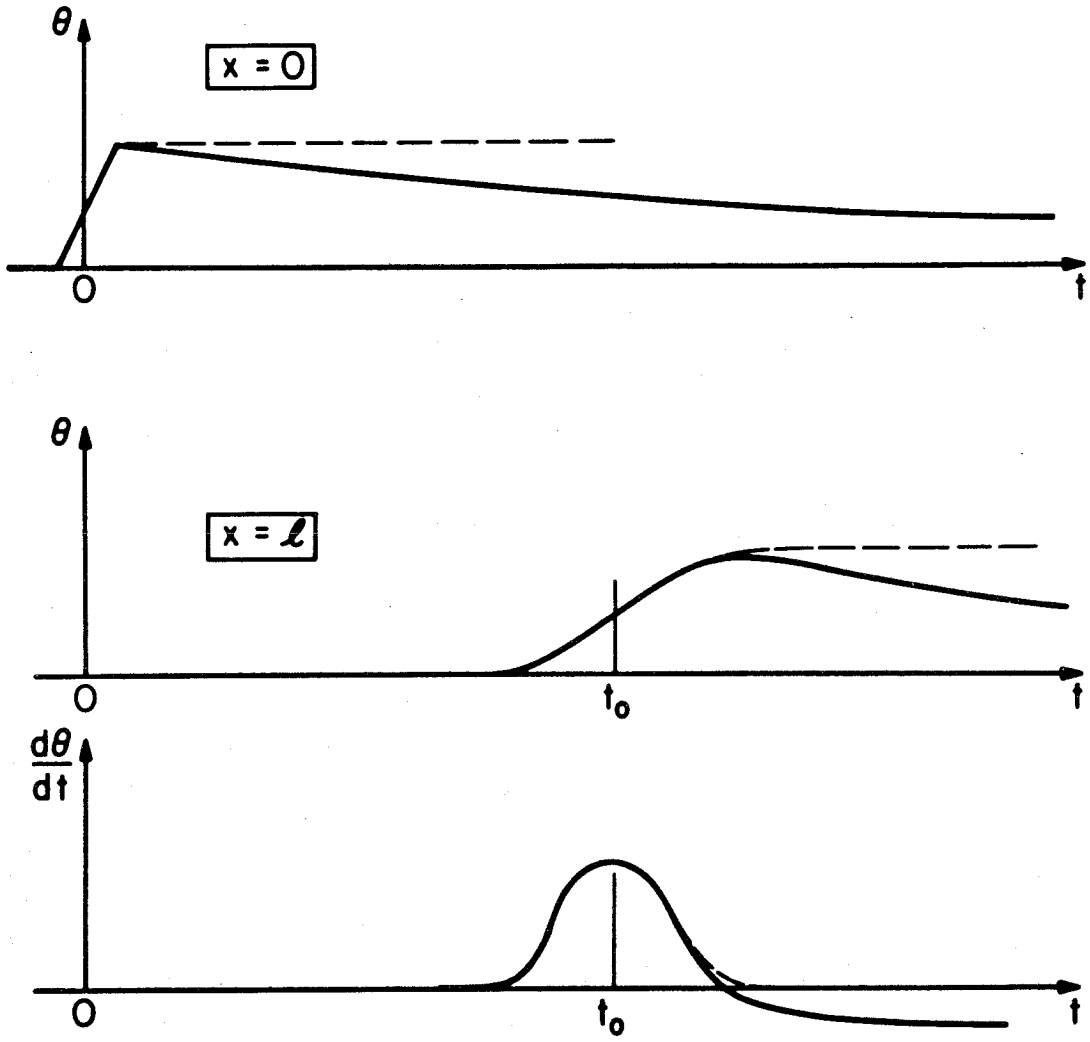

Figure 2. Ideal behavior of a ramp temperature rise in a uniform stream.

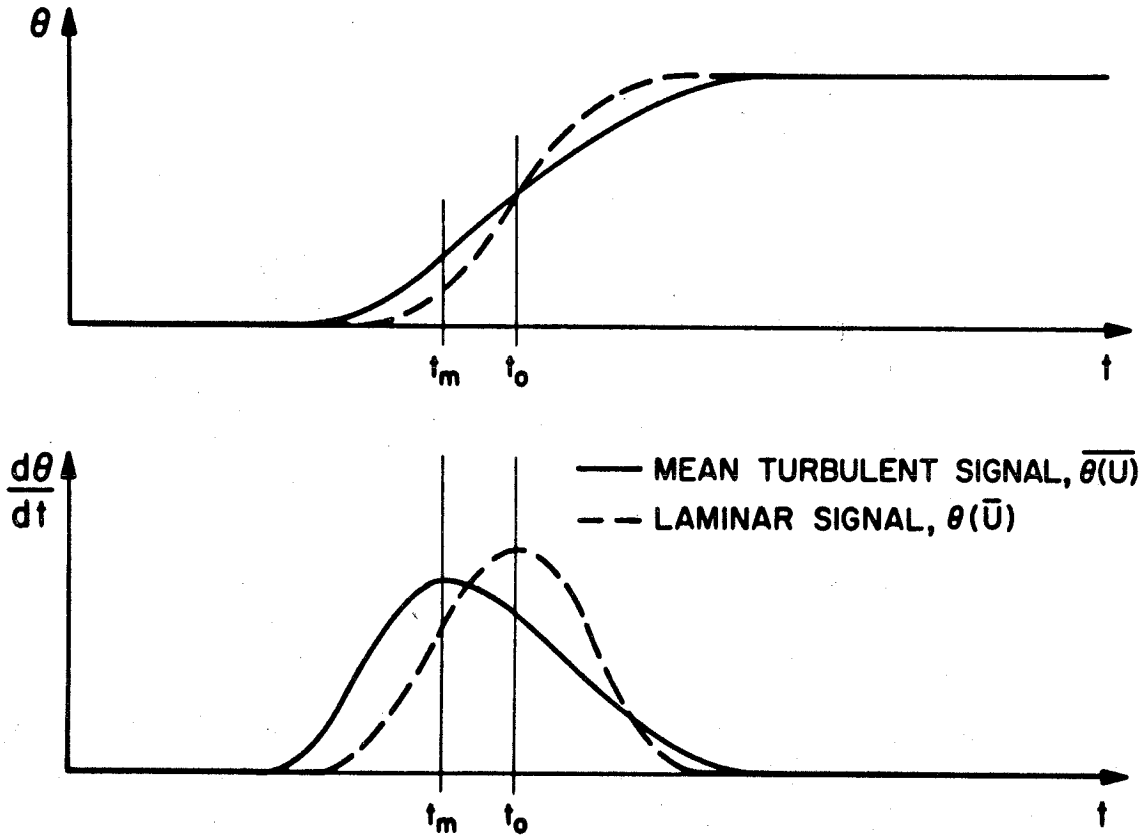

Figure 3. Effect of velocity fluctuations on the temperature profile shape.

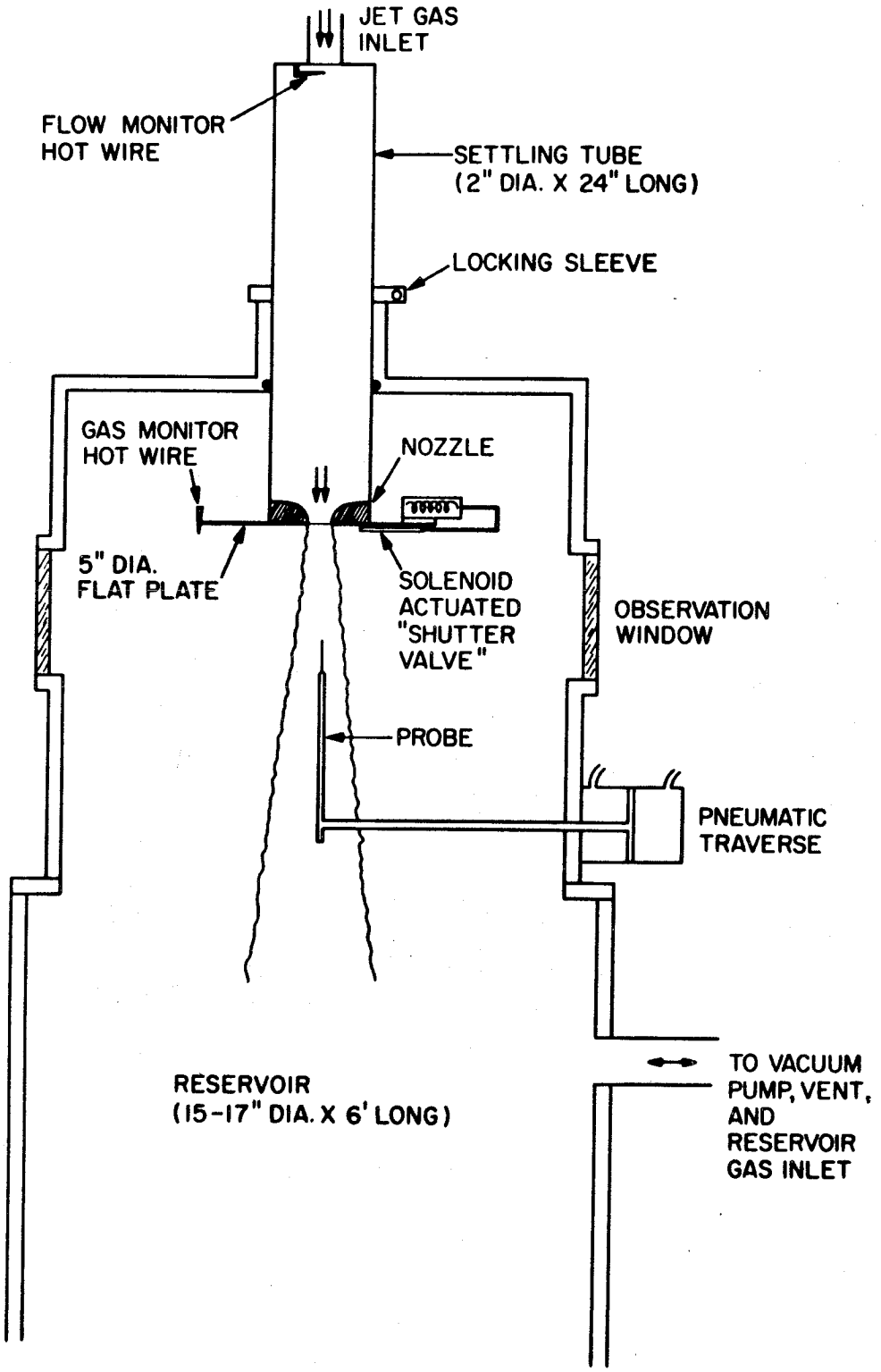

Figure 4. The experimental apparatus.

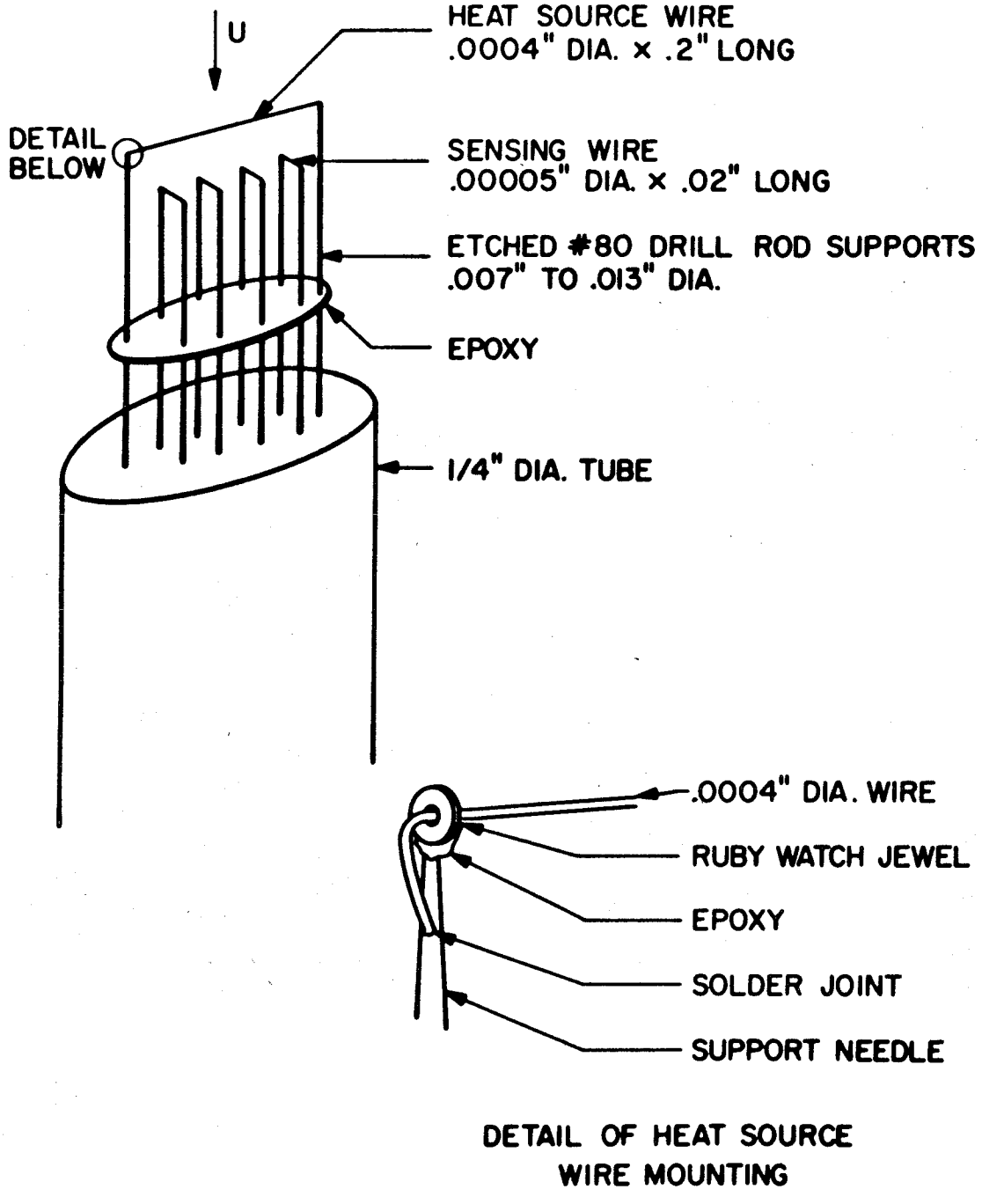

Figure 5. Probe Construction.

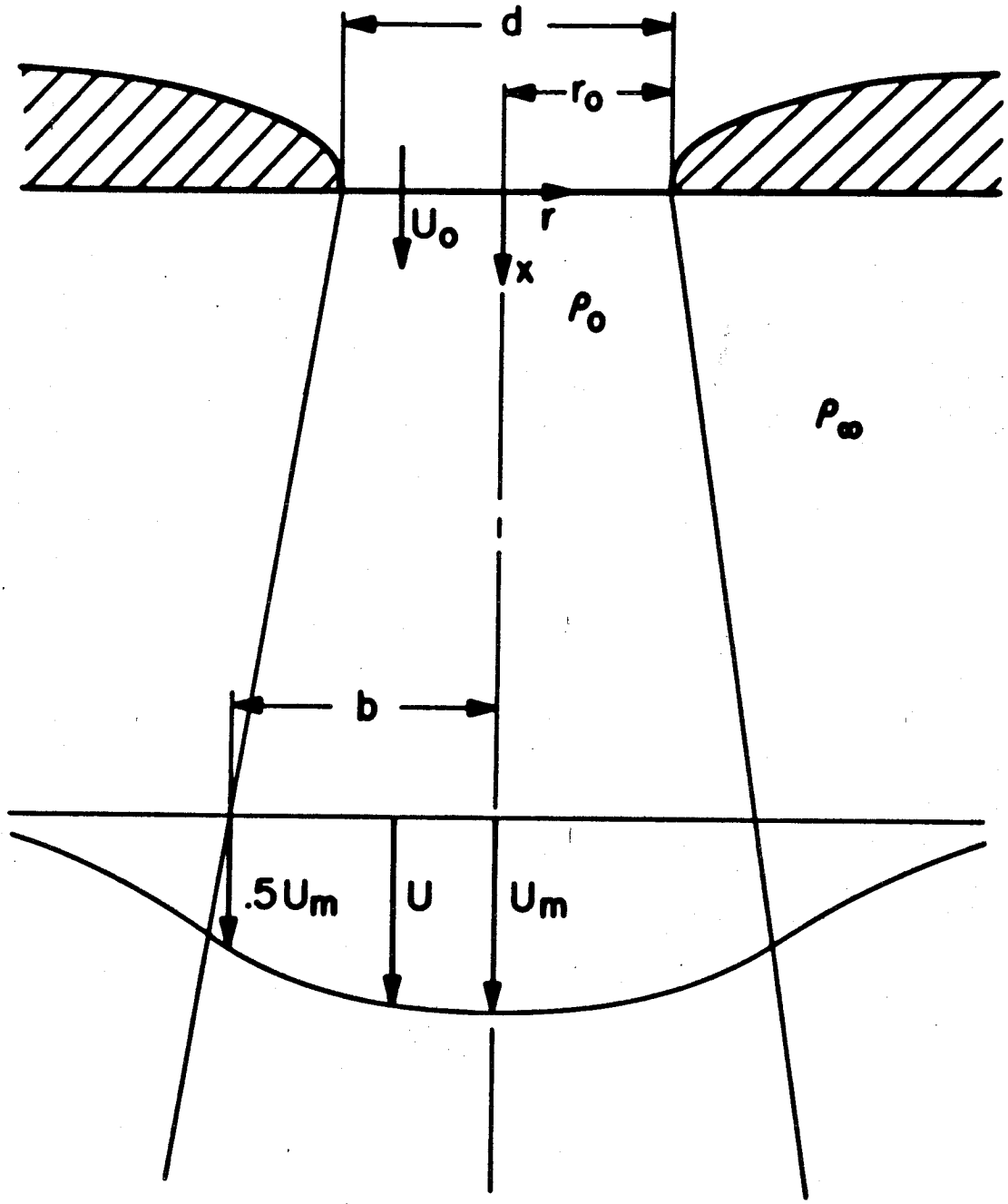

Figure 6. Definition of coordinates.

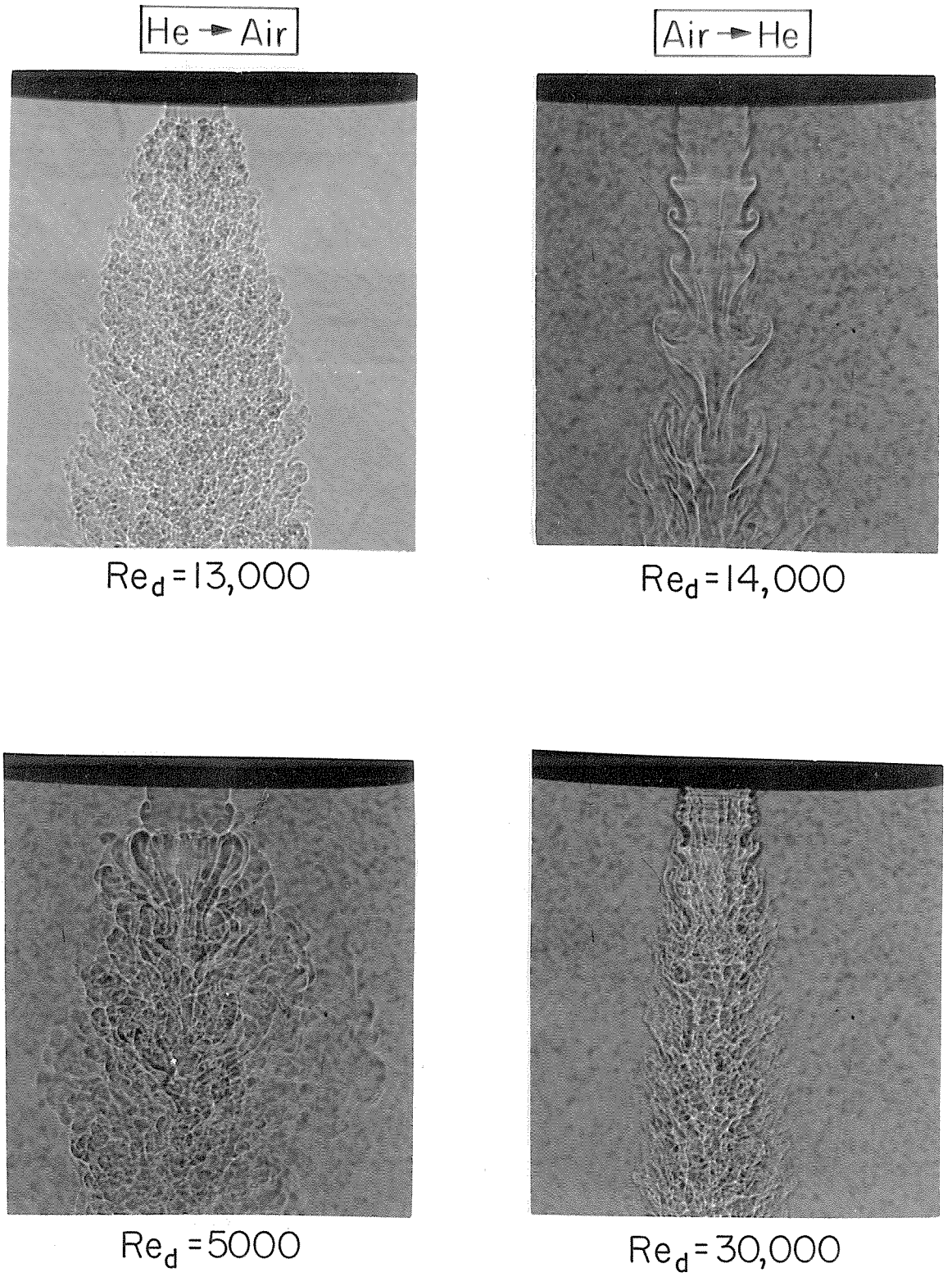

Figure 7. Shadow photographs of flow.

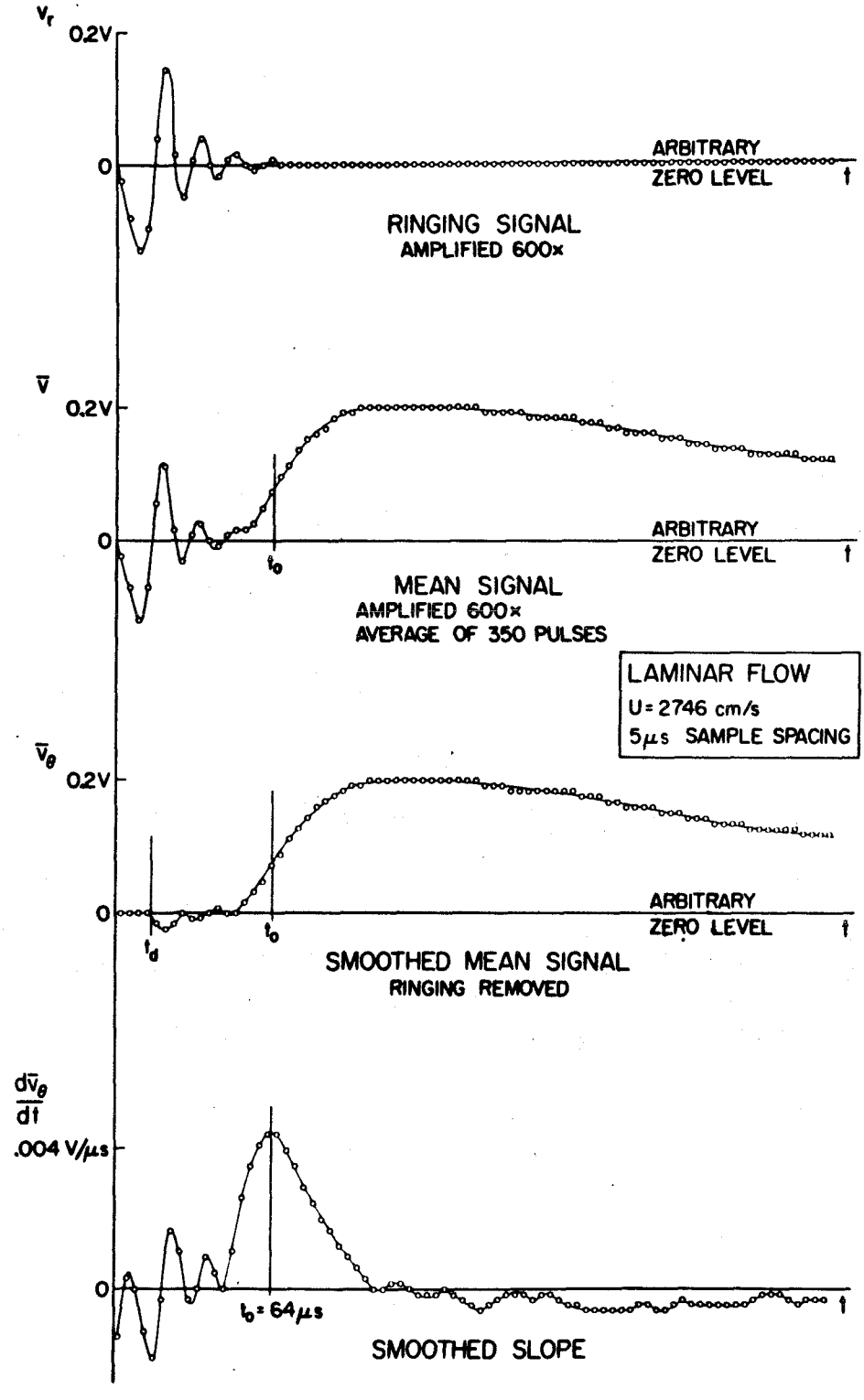

Figure 8. Computer plots of digitized sensing wire signal for laminar flow.

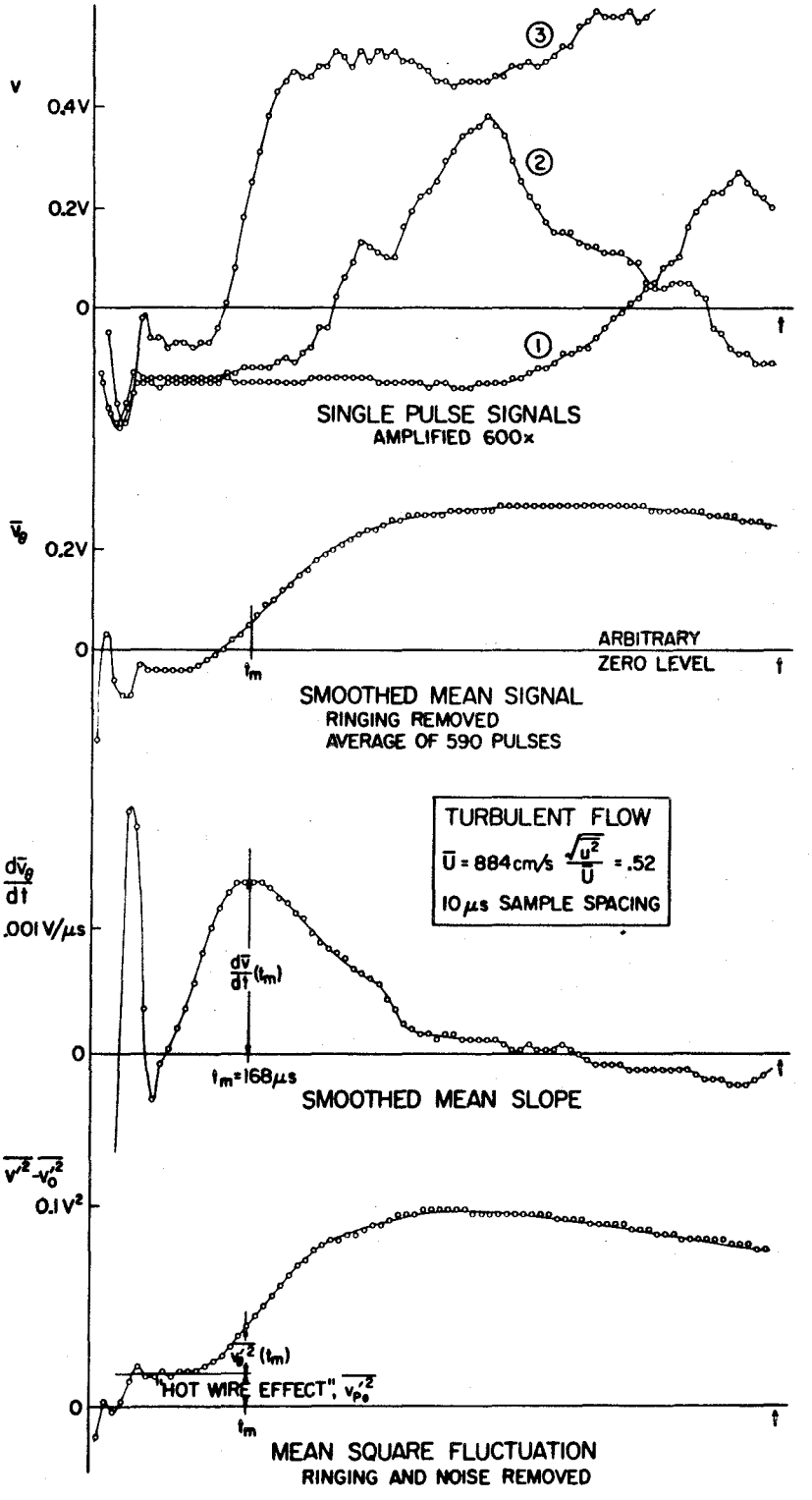

Figure 9. Computer plots of digitized sensing wire signal for turbulent flow.

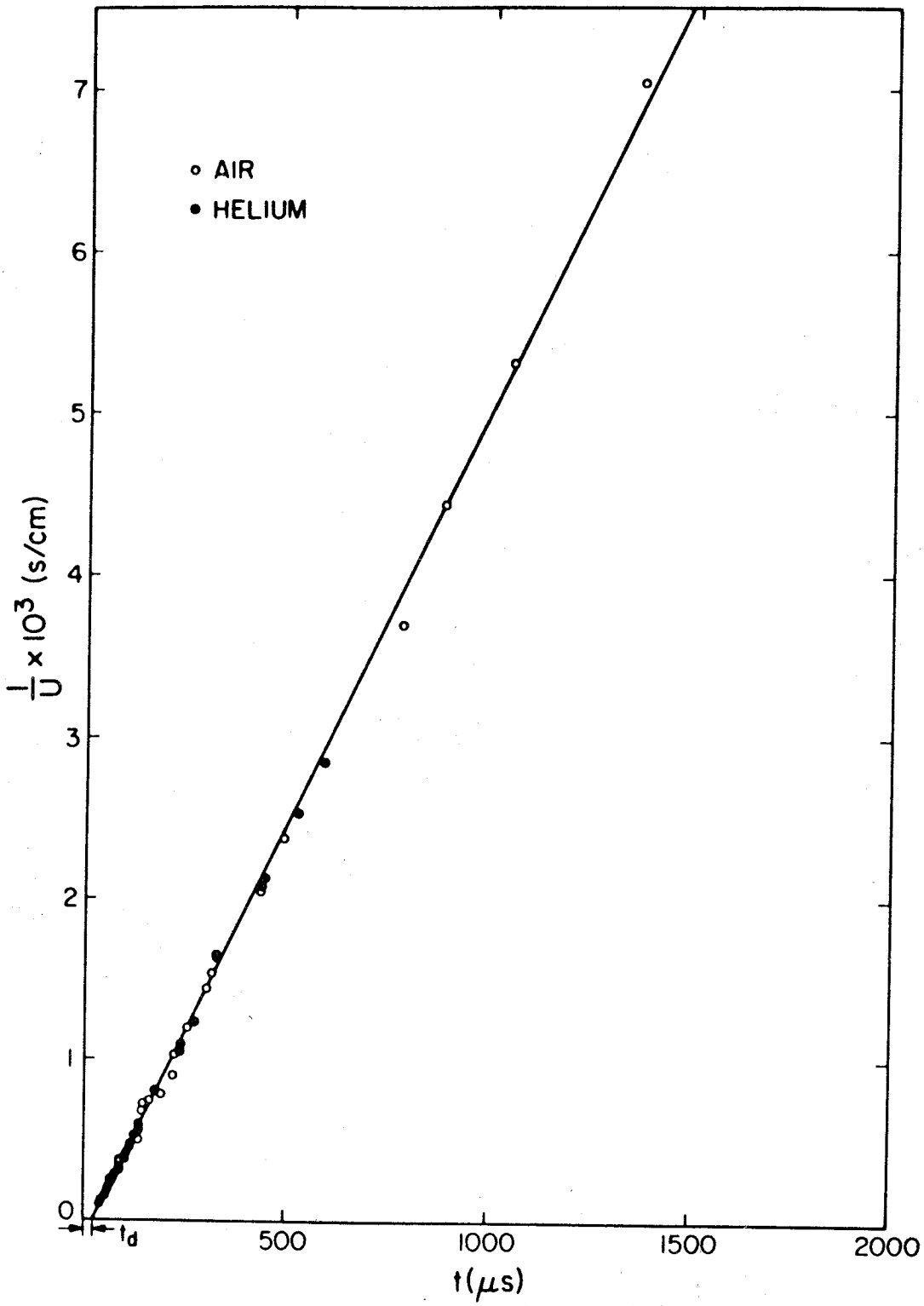

Figure 10. Typical probe calibration curve, showing effect of amplifier response time.

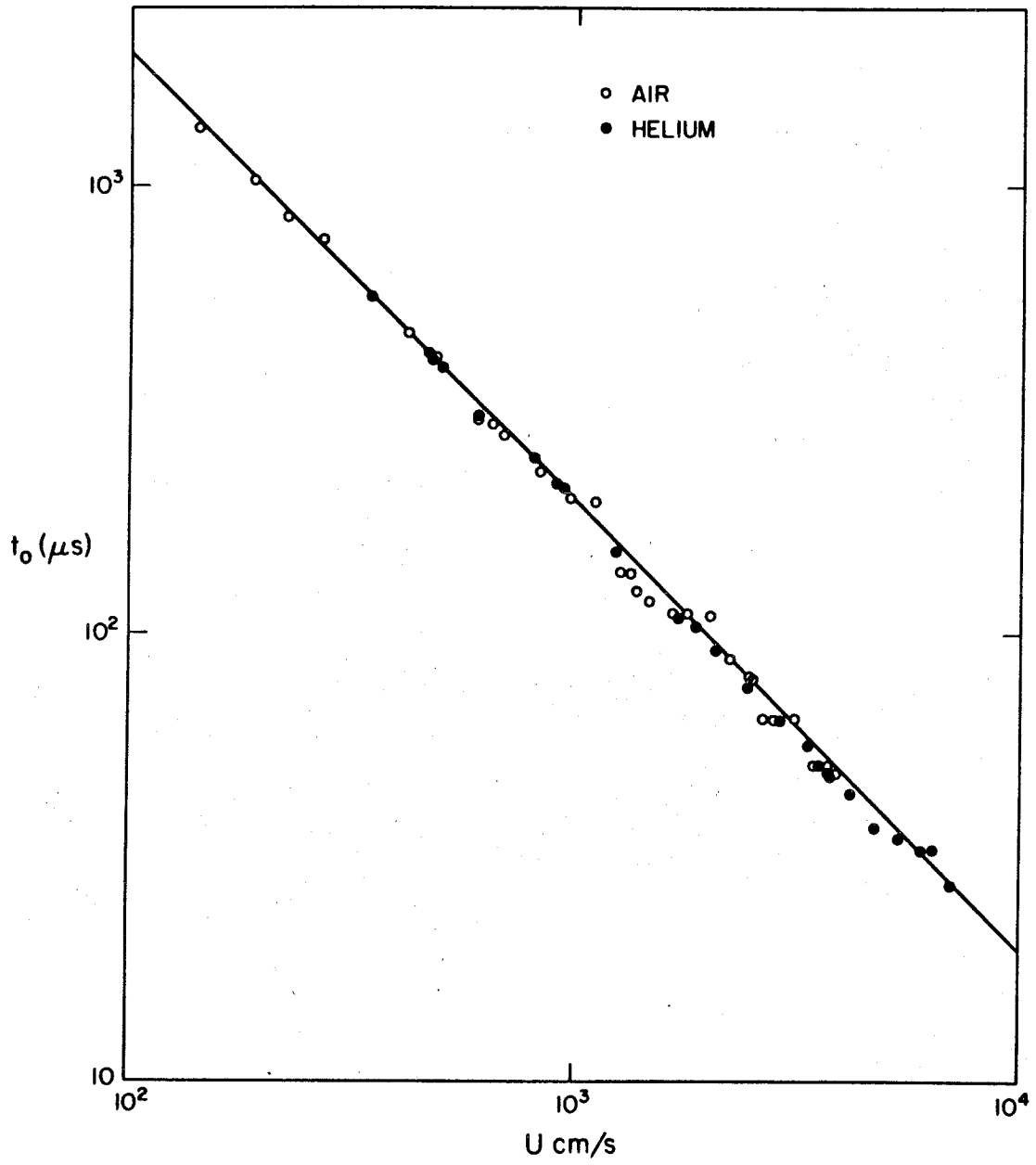

Figure 11. Typical probe calibration curve.

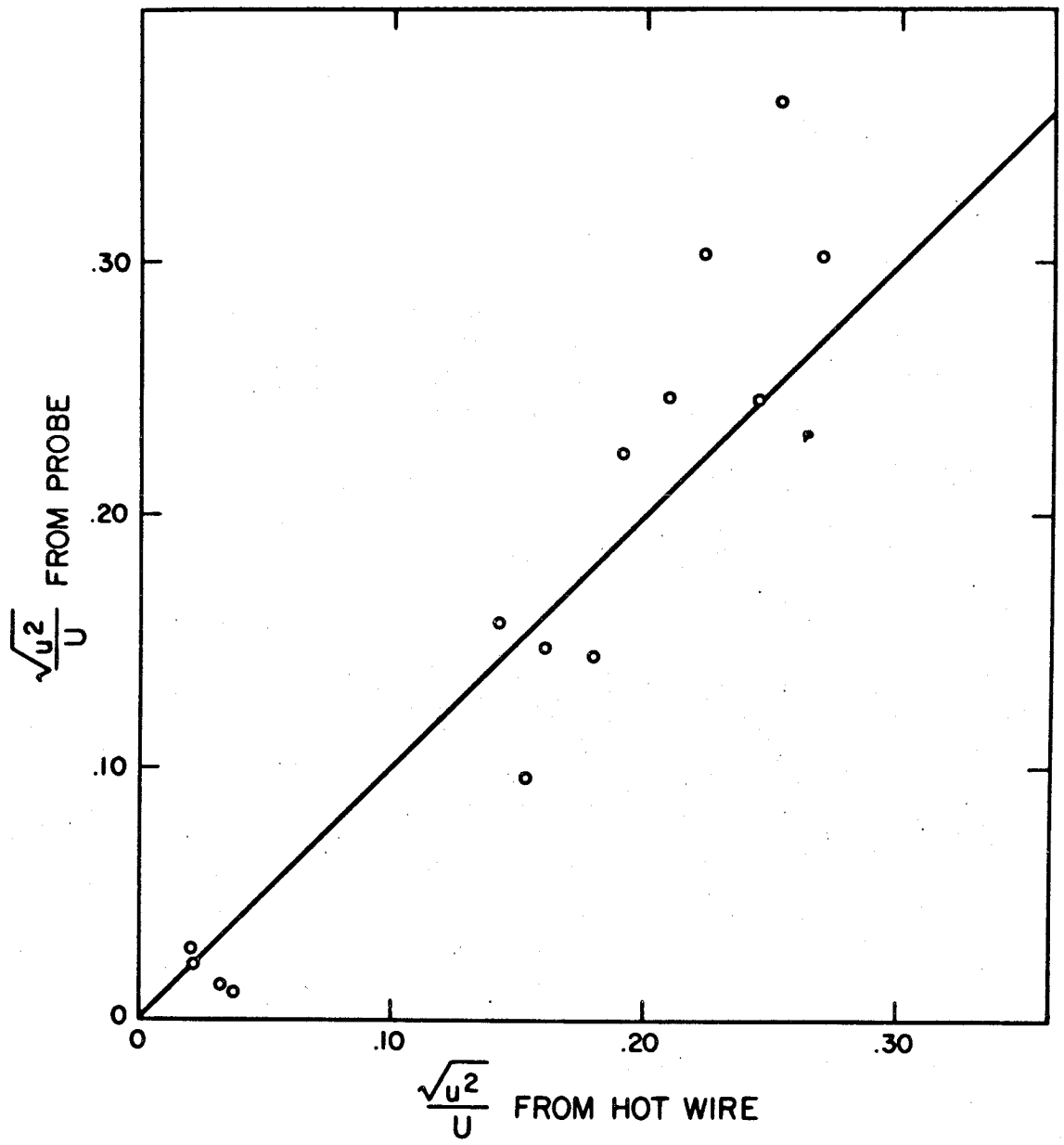

Figure 12. Comparison of fluctuation levels measured by the probe and by a linearized hot wire.

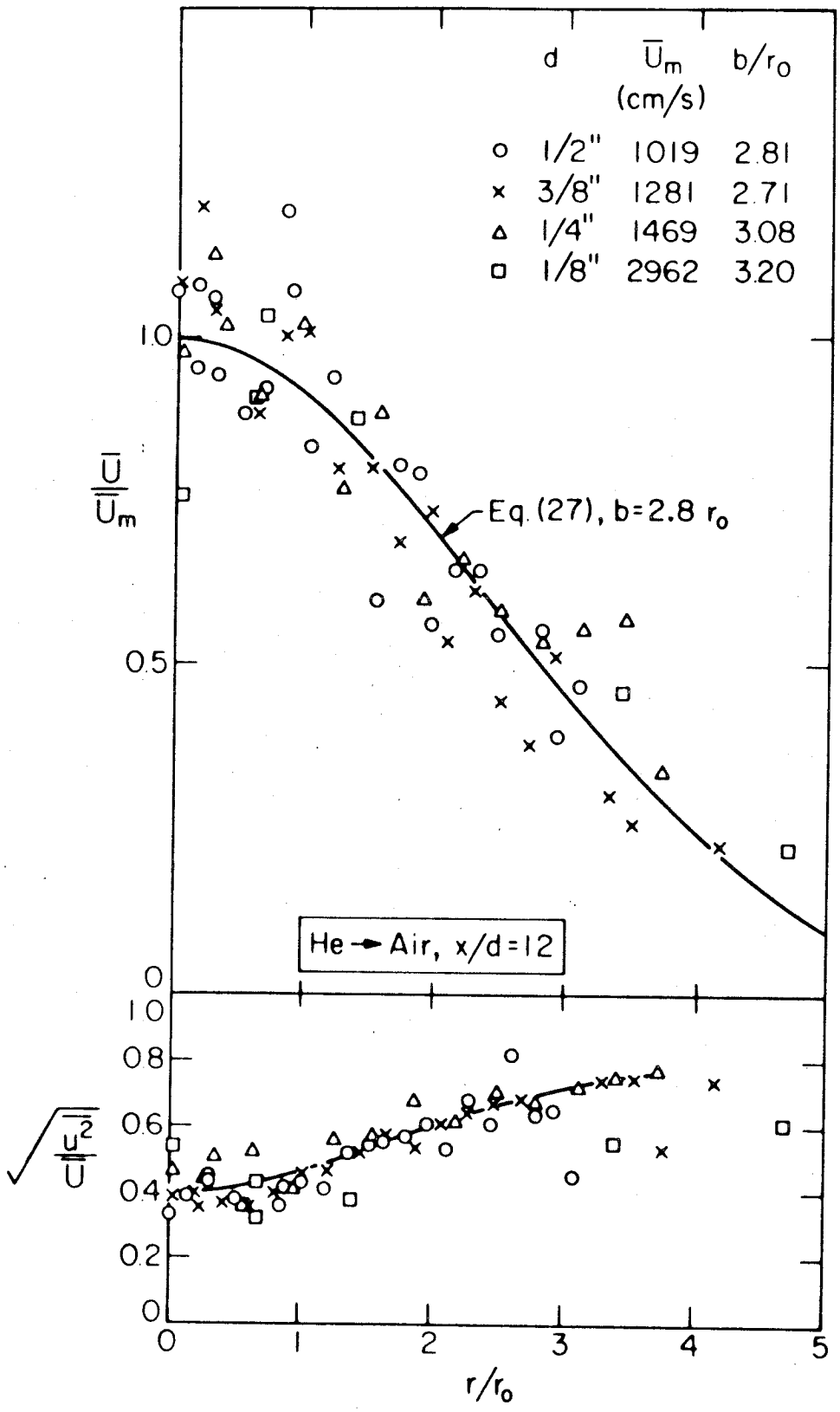

Figure 13. Typical radial profiles of the mean velocity and fluctuation level.

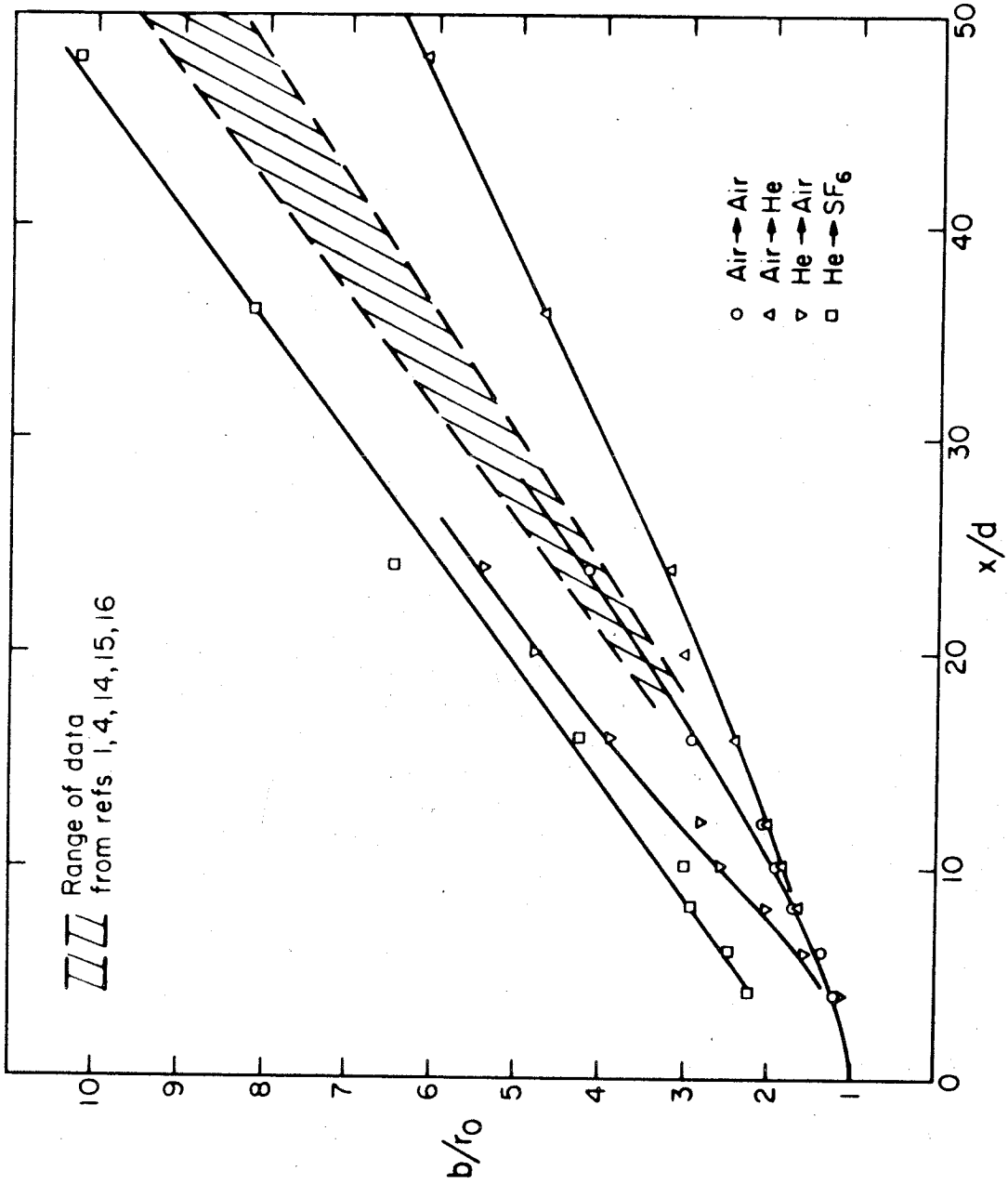

Figure 14. Axial variation of jet widths.

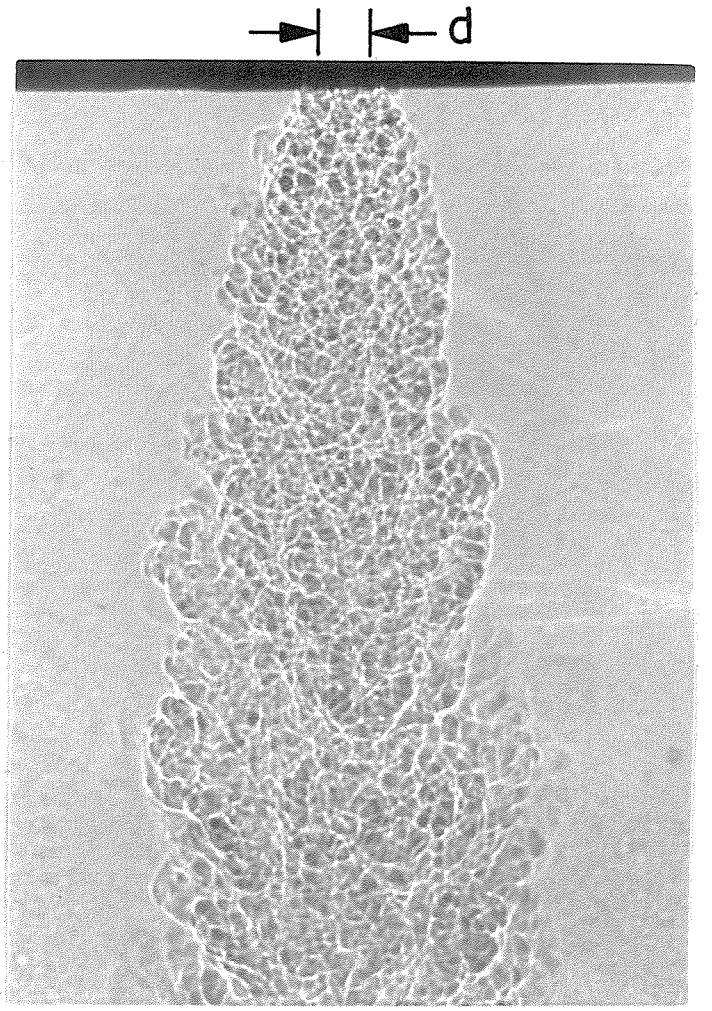

Figure 15. Shadow photograph of helium jet flowing into SF_6.

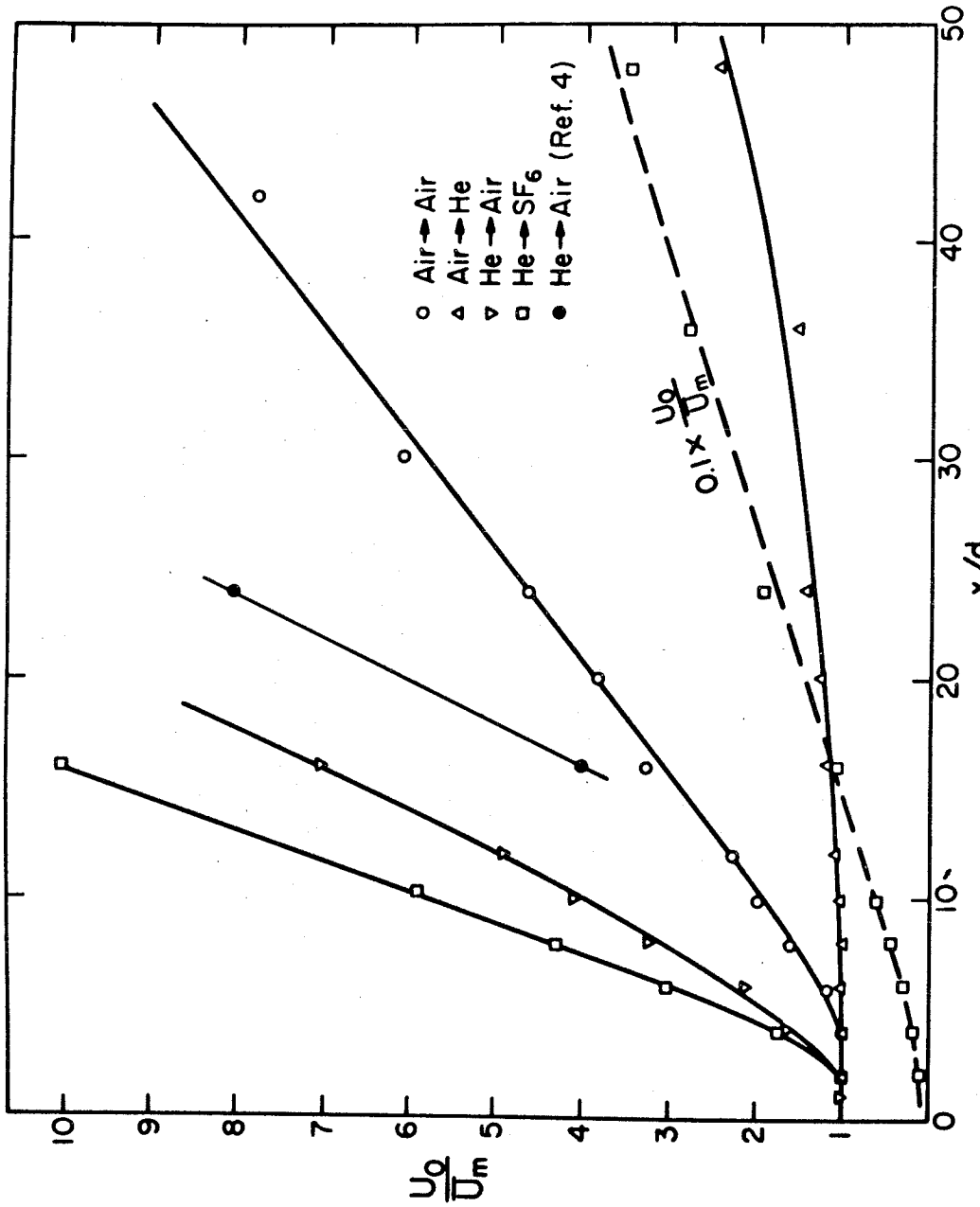

Figure 16. Axial velocity profiles.

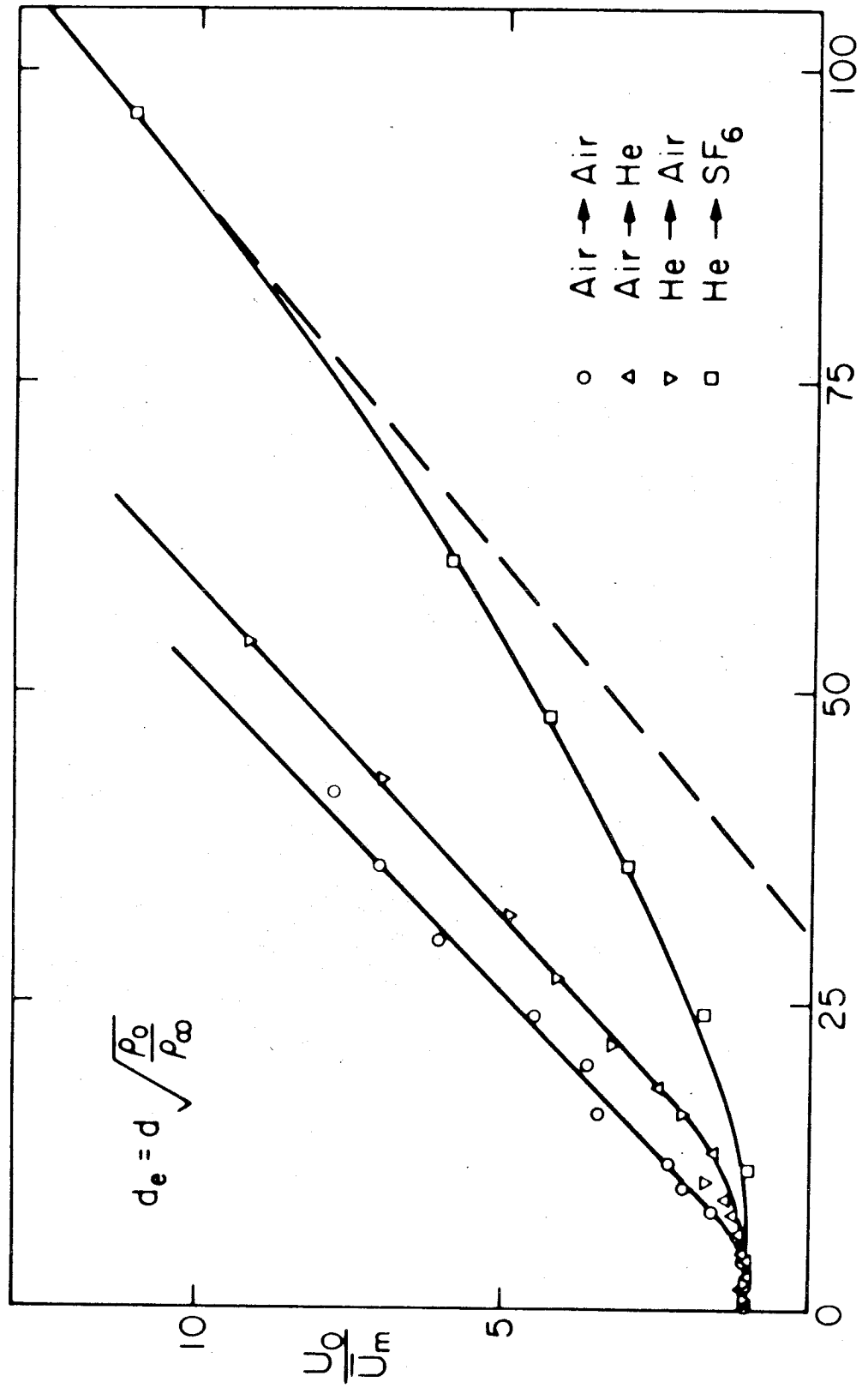

Figure 17. Axial velocity variation as a function of a density-scaled distance.

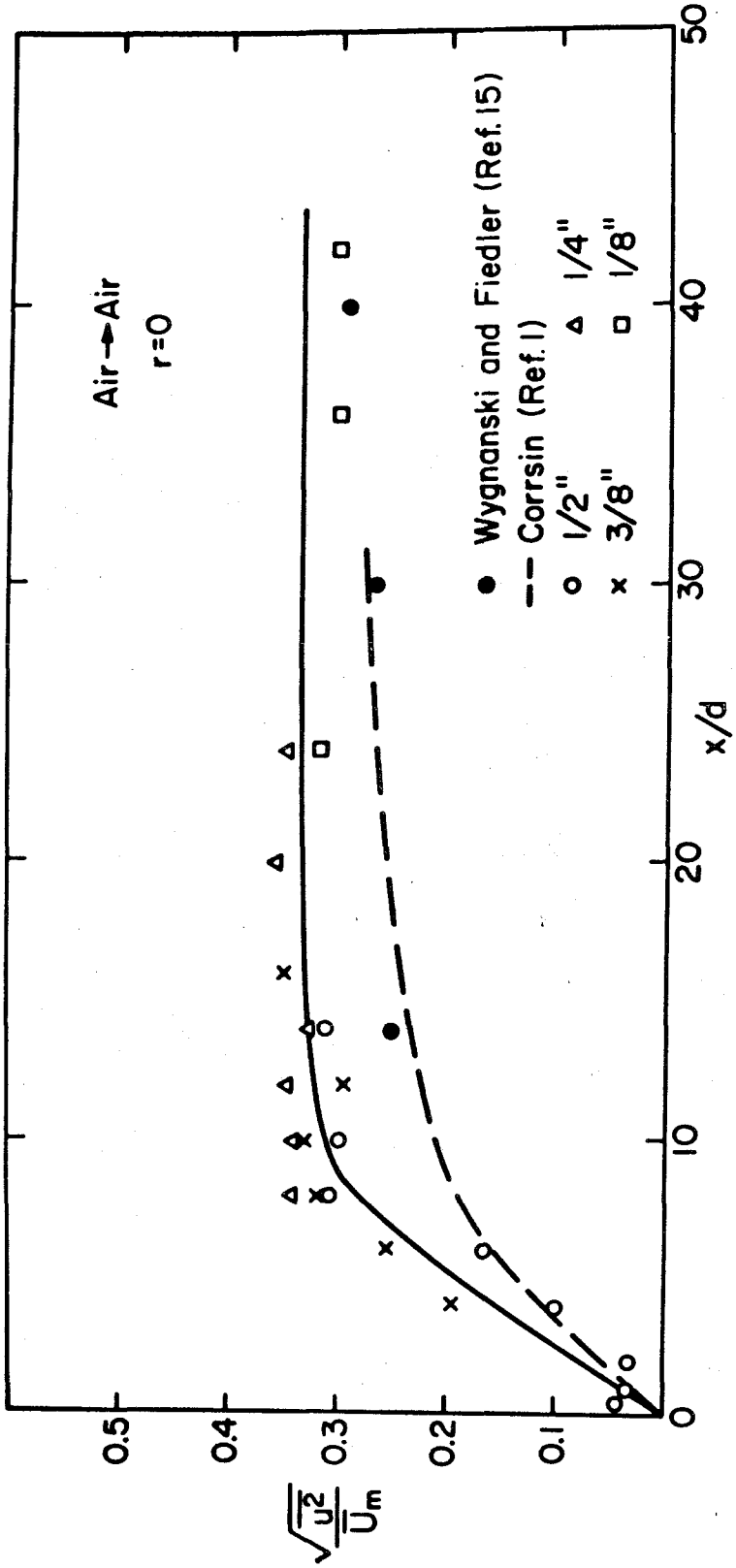

Figure 18. Axial variation of the centerline velocity fluctuation level in the homogeneous jet.

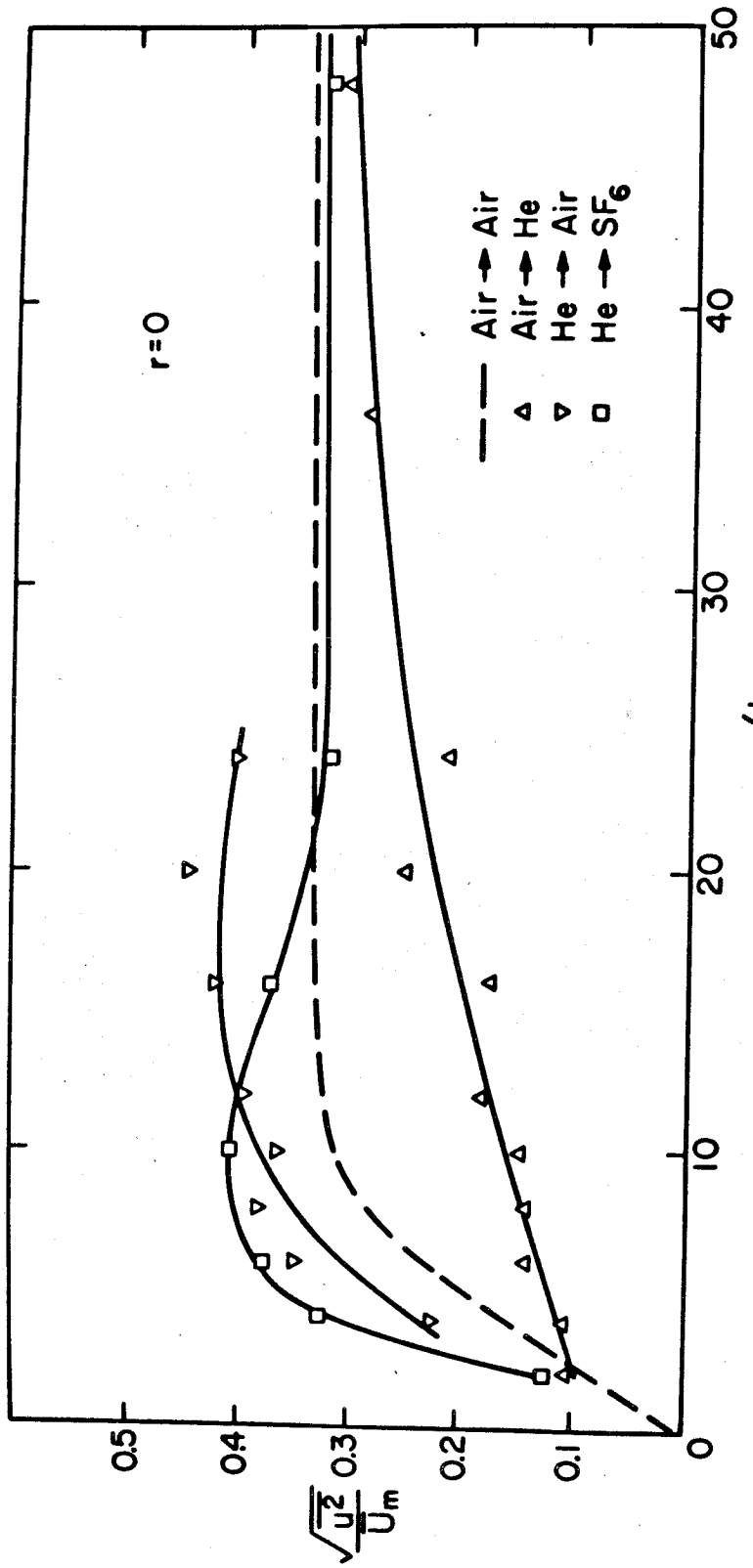

Figure 19. Axial variation of the centerline velocity fluctuation levels.